Discovery of a pyrazolopyridine alkaloid inhibitor of ERO1A that mitigates neuronal ER stress and age-related decline

Salinee Jantrapirom[1,2#], Apiwat Sangphukieo[2#], Natsinee U-on[2], Pattaporn Poonsawas[3], Wasinee Wongkumool[2], Ranchana Yeewa[2], Luca Lo Piccolo[2*]

Affiliations:

[1] Department of Pharmacology, Faculty of Medicine, Chiang Mai University, Chiang Mai, Thailand
[2] *Drosophila* Centre for Human Diseases and Drug Discovery (DHD), Faculty of Medicine, Chiang Mai University, Chiang Mai, Thailand
[3] Center of Multidisciplinary Technology for Advanced Medicine (CMUTEAM), Faculty of Medicine, Chiang Mai University, Chiang Mai, Thailand
[4] Faculty of Pharmaceutical Sciences, Khon Kaen University, Khon Kaen, Thailand

[#] These authors contributed equally to this work.
[*] Correspondence to: lopiccolo.l@cmu.ac.th

Keywords: ER-stress, ERO1A, natural products, UBQLN2, Amyotrophic Lateral Sclerosis, aging, pyridine alkaloid, human neuronal cells, *Drosophila*.

Abstract

Targeting Endoplasmic Reticulum Oxidoreductase 1 Alpha (ERO1A) offers therapeutic potential for ER stress-related conditions, including motor neurone diseases and congenital muscle disorders. However, selective ERO1A inhibitors remain unavailable. Here, we developed a multi-modal discovery pipeline combining molecular docking with *in vitro* and *in vivo* assays, screening 401,824 natural products from the COCONUT database. We identified two compounds, S88 and geniposide, that inhibited ERO1A *in vitro*, reduced tunicamycin-induced ER stress markers in human neurons, and improved locomotion and neuromuscular junctions in UBQLN2^{ALS} *Drosophila*. S88 maintained efficacy in late-stage disease and extended lifespan in a D-galactose aging model. In fly brains, S88 selectively reduced phosphorylated eIF2α without lowering its downstream effector ATF4, suggesting engagement of alternative mechanisms preserving ATF4 homeostasis. These findings highlight S88 as a promising lead for treating ER stress-associated neuromuscular disorders and demonstrate the utility of this integrative discovery pipeline for identifying bioactive natural compounds with disease-modifying potential.

Introduction

Endoplasmic reticulum (ER) stress is a hallmark of several neurodegenerative diseases, including Amyotrophic Lateral Sclerosis (ALS), and plays a crucial role in aging-related neuronal dysfunction [1-3]. The accumulation of misfolded proteins in the ER disrupts cellular homeostasis, triggering the unfolded protein response (UPR). While the UPR initially functions as a protective mechanism to restore ER balance, its prolonged activation contributes to neuronal cell death and disease progression. Thus, targeting ER stress pathways represents a promising therapeutic strategy for neurodegenerative diseases and age-related neuronal decline [4].

Among the regulators of ER stress, the Endoplasmic Reticulum Oxidoreductin 1 (ERO1) plays a crucial role in oxidative protein folding and maintaining redox balance. Its activity directly influences the burden of misfolded proteins in the ER, making it a critical factor in UPR activation [5-7]. While ERO1 is essential in yeast and worms, partial inhibition enhances survival under ER stress and even extends lifespan in worms and *Drosophila* [8-11]. In mammals, the presence of two isoforms, ERO1A and ERO1B, allows for functional flexibility, with loss-of-function mutations causing only mild defects [12-14]. Collectively, these findings support the hypothesis that targeted inhibition of ERO1 could offer therapeutic benefits in conditions characterized by maladaptive ER stress.

Notably, ERO1 inhibition has long been recognized as a potential anti-cancer strategy, given that many tumors exploit ER stress for survival and therapy resistance [15-17]. More recently, we and others have demonstrated the therapeutic potential of targeting ERO1A in non-cancerous diseases. Suppressing ERO1A, either genetically or pharmacologically with EN460 or the pan-ER stress inhibitor TUDCA, has shown beneficial effects in a *Drosophila* model of UBQLN2-ALS as well as in both *in vitro* and *in vivo* models of SEPN1-related myopathy (SEPN1-RM) [11,18]. This expanding therapeutic relevance underscores the importance of developing highly selective and low-toxicity ERO1 inhibitors, which could have broad applications in treating ER stress-related diseases beyond cancer.

Currently available ERO1A inhibitors, such as EN460, suffer from poor selectivity and potential off-target effects due to structural similarities with other FAD-containing enzymes, including MAO-A, MAO-B, and LSD1 [14,19]. Previous efforts to identify selective ERO1A inhibitors through virtual screening have led to candidates with improved binding affinity. However, the lack of comprehensive profiling against other FAD enzymes, along with challenges in bioavailability and metabolic stability, may limit their sustained inhibitory effects and potential therapeutic applications [20,21].

Natural products have become valuable source for developing new lead compounds and scaffolds due to their diversity of biological activities and drug-like properties [22,23]. Therefore, in this study, we employed a multi-modal strategy structure-based virtual docking with *in vitro* and *in vivo* assays to identify novel natural small-molecule inhibitors of ERO1A with improved specificity and translational potential. Among 401,824 natural products screened, we identified the heterocyclic alkaloid CNP0410364 (hereafter referred to as S88) as a potent ERO1A inhibitor with promising neuroprotective effects.

S88 consistently attenuated the unfolded protein response (UPR) across species and improved neuronal survival in both human neurons under tunicamycin-induced stress and in *Drosophila* models of motor neurone disease (UBQLN2^{ALS}), which recapitulates chronic ER stress caused by proteostasis dysfunction. *In vivo*, S88 preserved *Drosophila* UBQLN2^{ALS} locomotor function across disease progression, maintaining efficacy even at late stages, where other compound candidates failed. Furthermore, S88 extended lifespan in a *Drosophila* model of accelerated aging induced by D-galactose (D-GAL), indicating broader protective effects.

These results underscore the therapeutic relevance of ERO1A inhibition and position S88 as a tractable small molecule for further investigation in ER stress–associated neurodegenerative and age-related disorders.

Material and Methods

Phytochemical compound virtual screening.

The three-dimensional (3D) structure of ERO1A was obtained from the Protein Data Bank (PDB) under accession ID 3AHQ, while the structure of ERO1B was predicted using SWISS-MODEL [24] using ERO1A as the template. The 3D structures of other FAD-containing enzymes, MAO-A, MAO-B, and LSD1, were retrieved from the PDB under accession IDs of 2Z5X, 2V5Z, and 6W4K, respectively. For all structures, non-protein molecules such as water, sodium, and magnesium ions were removed from the PDB files to retain only the protein molecules. Phytochemical compounds were obtained from the COCONUT database, consisting of 401,824 unique compounds. Initial filtering was based on drug-likeness properties, including a fraction of sp3 carbon atoms (Fsp3) > 0.4, lipophilicity (xlogp) < 5, and molecular weight (MW) < 500 Daltons. 3D structures (PDB format) of the passed compounds were generated from their SMILES format (smi) using Gypsum v1.2.0 [25]. Python scripts, prepare_ligand4.py and prepare_receptor4.py from AutoDockTools [26], were used to convert PDB file of both ligands and protein targets into pdbqt format. A grid box was then set to cover the FAD-binding site on each protein target. Molecular docking simulations were conducted using AutoDock Vina [27] with an exhaustiveness setting of 8 to predict binding energy between ligands and protein targets. The lowest binding energy for each ligand was used to identify the most favorable docking pose. To evaluate the binding affinity of FAD-containing enzymes and their known inhibitors, the inhibitors from their original PDB files were removed and re-docked to their relevant protein targets using the same procedure. The binding affinity of these known inhibitors was used as a cutoff, and phytochemical compounds showing a binding affinity at least 1 kcal/mol lower than the inhibitors were considered to have favorable binding ability to the target.

Compound handling and preparation

All chemicals were initially prepared as concentrated stock solutions in 100% DMSO and subsequently diluted to working concentrations, except for D-galactose (D-GAL). Retinoic acid (Sigma-Aldrich, CAS No. R2625) and tunicamycin (Sigma-Aldrich, CAS No. 11089-65-9) were prepared as 100 mM and 5 mg/mL stock solutions, respectively. The phytochemicals CNP0392367 (CAS No. STL522543), CNP0168092 (CAS No. STL551047), CNP0392367 (CAS No. STK179676), and CNP0162092 (CAS No. STL546888) were obtained from Vitas-M Laboratory (Hong Kong), and geniposide (CAS No. T2212) was purchased from TargetMol. All phytochemicals were prepared as 20 mM stock solutions in DMSO. Additional details on phytochemicals are provided in Supplementary Tables S1–S4. D-GAL was directly dissolved in the *Drosophila* culture medium at final concentrations of 25 mg/mL and 30 mg/mL. The compounds utilized in this study, along with their CAS registry numbers, are listed in Supplementary Table S7 unless otherwise specified.

In vitro ERO1L enzymatic activity and inhibition assay

The enzymatic activity of recombinant human ERO1L (rhERO1L, MedChemExpress, cat: HY-P70893) and the inhibitory effects of selected phytochemicals were evaluated *in vitro* using the Amplex® Red Hydrogen Peroxide/Peroxidase Assay Kit (Invitrogen, A22188), which includes Amplex® Red reagent, anhydrous dimethylsulfoxide (DMSO), horseradish peroxidase (HRP), and hydrogen peroxide (H_2O_2). Reactions were performed in the presence of cell-derived human PDI (hPDI, SinoBiological, cat: 10827-H08H). Reaction mixtures contained rhERO1L (10 ng/μL), hPDI (10 ng/μL), H_2O_2 (10 μM), HRP (0.1 U/mL), Amplex® Red (25 μM), and either phytochemicals (100 μM) or EN460 (25 μM, EMD Millipore) as a reference inhibitor, in 0.25 M sodium phosphate buffer (pH 7.4). Reactions were prepared in black, flat-bottom 96-well plates (SPL Life Sciences, Korea) and incubated at room temperature. Fluorescence was measured every 10 minutes over a 30-minute period using an Infinite® M Plex multimode microplate reader (Tecan Trading AG, Switzerland) with excitation at 544 nm and emission at 590 nm (top read). Fluorescence intensity from ERO1L/PDI reactions without inhibitors after 10 minutes of incubation was defined as 100% activity. Relative enzymatic activity in the presence of each phytochemical or EN460 was calculated accordingly.

Measurement of radical scavenging activity

The antioxidant capacity of selected phytochemicals was evaluated using two complementary assays that measure radical scavenging activity via different chemical mechanisms and solvent environments. The 1,1-diphenyl-2-picrylhydrazyl (DPPH) assay assesses the ability of compounds to neutralize lipophilic free radicals in methanolic solution, while the 2,2′-azino-bis(3-ethylbenzothiazoline-6-sulfonic acid) radical cation (ABTS) assay evaluates both hydrophilic and lipophilic antioxidant activity by measuring the reduction of a stable radical cation in aqueous conditions. For the DPPH assay, a 0.2 mM DPPH solution was freshly prepared in methanol. Test reactions were performed in 96-well plates according to the previously established protocol [28] by mixing 180 μl of the DPPH solution with 20 μl of each phytochemical dissolved in methanol at the indicated concentrations. Methanol alone (20 μl) was used as a negative control. Reactions were incubated at room temperature in the dark for 30 minutes, and absorbance was measured at 517 nm. Trolox, n-acetylcysteine and ascorbic acid served as positive controls. The percentage of DPPH radical scavenging was calculated after correcting for the intrinsic absorbance of the test compounds:

$$\%\ of\ DPPH\ radical\ scarvenging\ activity = \left(\frac{\left(A_0 - A_{0\,(c)}\right) - \left(A_t - A_{t\,(c)}\right)}{\left(A_0 - A_{0\,(c)}\right)}\right) x\ 100$$

The absorbance of the control (A_0) was corrected by subtracting the absorbance of methanol only ($A_{0\ (c)}$), and the absorbance of either tested phytochemicals or standards (A_t) was corrected by subtracting the absorbance of methanol mixed with the tested compounds ($A_{t\ (c)}$). Each compound was tested in triplicate across independent experiments (n ≥ 3).

For the ABTS assay, ABTS radical cations (ABTS$\bullet^+$) were generated by mixing equal volumes of 7 mM ABTS and 2.45 mM potassium persulfate, followed by incubation in the dark at room temperature for 12–16 hours, as described in [29]. The resulting ABTS$\bullet^+$ solution was diluted 1:30 in Milli-Q water to achieve an absorbance of 0.70 ± 0.10 at 734 nm. In 96-well plates, 180 µl of diluted ABTS$\bullet^+$ solution was mixed with 20 µl of each test compound or control (dissolved in MQ water). After 6 minutes of incubation in the dark at room temperature, absorbance was measured at 734 nm. Trolox, n-acetylcysteine and ascorbic acid were used as positive controls. The percentage of scavenging inhibition was calculated using the following formula:

$$\%\ of\ ABTS\ radical\ scarvenging\ activity = \left(\frac{\left(Abs_0 - Abs_{0\,(c)}\right) - \left(Abs_t - Abs_{t\,(c)}\right)}{\left(Abs_0 - Abs_{0\,(c)}\right)}\right) x\ 100$$

The absorbance of the control (A_0) was corrected by subtracting the absorbance of methanol only ($A_{0\ (c)}$), and the absorbance of either tested phytochemicals or standards (A_t) was corrected by subtracting the absorbance of methanol mixed with the tested compounds ($A_{t\ (c)}$). All measurements were performed in triplicate and repeated in at least three independent experiments.

Human skin dermis-derived fibroblasts isolation

A skin biopsy was obtained from a healthy donor following a protocol approved by the Ethical Committee of the Faculty of Medicine, Chiang Mai University, under study code PED-2566-0380. A punch biopsy was collected and immediately placed in a 50 mL conical tube containing 10 mL of Dulbecco’s Modified Eagle Medium (DMEM; Gibco, Thermo Fisher Scientific, Waltham, MA, USA) supplemented with 1% penicillin-streptomycin (pen-strep; HyClone, Cytiva, Marlborough, MA, USA) to prevent contamination. Under sterile conditions, the biopsy was transferred into a digestion medium composed of DMEM, 20% fetal bovine serum (FBS; Sigma-Aldrich, St. Louis, MO, USA), collagenase type I (Gibco, Thermo Fisher Scientific, Cat# 17100-017), and 1% pen-strep. The tissue was incubated overnight at 37°C to facilitate enzymatic digestion. The following day, the sample was thoroughly mixed to promote epidermal separation and dermal disintegration. The mixture was then centrifuged to obtain a cell pellet, which was subsequently resuspended in fibroblast culture medium consisting of DMEM supplemented with 20% FBS and 1% pen-strep. The suspension was plated into a T75 culture flask and incubated at 37°C with 5% CO_2 for 6–7 days to allow fibroblast attachment. After 7 days, fibroblast-like cells were observed. At this stage, the culture medium was replaced with fibroblast culture medium containing 10% FBS to promote cell proliferation. Once the culture reached 80% confluency, cells were passaged at a 1:3 ratio using 0.25% trypsin-EDTA (HyClone, Cytiva, Marlborough, MA, USA). Human-derived fibroblasts (HDF) were expanded up to passage 3 and cryopreserved in liquid nitrogen for long-term storage.

Cell culture

Hepatocellular carcinoma (HepG2, ATCC: HB-8065) and neuroblastoma (SH-SY5Y, ATCC: CRL-2266) cell lines were obtained from the American Type Culture Collection (ATCC, Manassas, VA, USA). The HepG2 cells were cultured in T25 flasks using Dulbecco's Modified Eagle Medium (DMEM) (Gibco, Grand Island, USA) supplemented with 10% fetal bovine serum (FBS) and 1% penicillin-streptomycin (both from Corning, USA). The SH-SY5Y cells were cultivated in T25 flasks using 1:1 mixture of Eagle's Minimum Essential Medium (EMEM) (ATCC, Manassas, VA, USA) and F-12 medium (Gibco, Grand Island, USA), supplemented with 10% fetal bovine serum (Corning, Woodland, CA, USA) and 1% penicillin-streptomycin (Corning, Manassas, VA, USA). Cultures were maintained at 37°C with 5% CO_2, and all experiments were performed using cells at passages 6–12. All experiments involving cell culture were approved by the Institutional Biosafety Committee (ICB) of the Faculty of Medicine, Chiang Mai University (Thailand), under protocol number CMUIBC0268022.

Neuronal differentiation of SH-SY5Y cells

To induce neuronal differentiation, SH-SY5Y cells were seeded in 6-well plates at 1 × 10^5 cells/well and cultured in EMEM/F-12 medium with 10% FBS for 24 hours. On day 0 (D0), differentiation was initiated by replacing the medium with differentiation medium containing 10 µM retinoic acid (RA) in EMEM/F-12 supplemented with 10% FBS. The RA-containing medium was refreshed every two days until day 5 (D5). Neuronal differentiation was confirmed by phase-contrast microscopy and Western blot analysis of neuronal marker expression.

Cell viability and cytotoxicity assay

Cell viability and cytotoxicity were assessed using the MTT assay (3-(4,5-dimethylthiazolyl-2)-2,5-diphenyltetrazolium bromide). The assay was used to evaluate (i) cell viability under tunicamycin (Tm)-induced ER stress, with or without phytochemical treatment, and (ii) the cytotoxic effects of the phytochemicals alone. For ER stress experiments, SH-SY5Y cells (either undifferentiated or differentiated with retinoic acid (RA) for 3 days) were used. Undifferentiated cells were seeded in 96-well plates at 2 × 10^4 cells/well and cultured for 24h before treatment with Tm at 0.1, 1, or 10 µM for 24 or 48 hours. Differentiated cells were seeded at 3.3 × 10^3 cells/well, maintained in RA until day 3, and treated with the same Tm concentrations and durations. To evaluate the cytotoxicity of the selected phytochemicals (S43, S47, S76, S88, and T2212), human dermal fibroblasts (HDF), HepG2, and SH-SY5Y cells were seeded in 96-well plates at 2.5 × 10^3, 5 × 10^3, and 2 × 10^4 cells/well, respectively. After 24h of culture in EMEM/F12 medium, cells were treated with increasing concentrations (1, 2.5, 5, 10, and 20 µM) of each compound for 24 or 48h. To assess the potential protective effects of the phytochemicals against Tm-induced ER stress, SH-SY5Y cells (undifferentiated or 3-day RA-differentiated) were treated with 10 µM or 20 µM of each compound following 24 hours of Tm exposure. Vehicle-treated cells (0.1% DMSO) served as controls. For the MTT assay, culture media were replaced with 0.5 mg/mL MTT solution (BioChemica, Barcelona, Spain), and cells were incubated for 4h at 37 °C. The MTT-containing medium was then discarded, and 100 µL of DMSO (Labscan, Bangkok, Thailand) was added to dissolve the resulting formazan crystals. Absorbance was measured at 570 nm using a microplate reader (SpectraMax ABS Plus, MOLECULAR DEVICES). Unless otherwise specified, each condition included six technical replicates across two biological replicates. Results were expressed as a percentage of viable cells relative to controls. For untreated controls, viability was normalized to cells not exposed to DMSO. For Tm- and phytochemical-treated samples, viability was normalized to DMSO vehicle controls at either 0.05% or 0.1%, as appropriate.

Drosophila **husbandry and stocks**

Drosophila melanogaster stocks were maintained on a standard cornmeal-yeast-glucose medium at 22°C with 60% humidity under a 12:12 light/dark cycle unless otherwise stated. The Gal4/UAS binary system [30] was used for targeted, tissue-specific knockdown or overexpression. Pan-neuronal knockdown or overexpression was achieved using the nSyb-GAL4 or elav-GAL4 drivers at 25°C. The glass multiple reporter (GMR)-GAL4 promoter was used for targeting transgene's expression to developing eyes at 28°C. The following transgenic fly lines were obtained from the Bloomington Drosophila Stock Center (BDSC): nSyb-GAL4 (#68222), elav-GAL4 (#8760), *UAS-dsRNA ERO1L* (#64674), *UAS-ERO1L* (#42698), *UAS-EGFP* (#5431), *UAS-AUG-DsRed* (#6282), *UAS-dsRNA green fluorescent protein* (*GFP IR*, #9330) and *UAS-HA-UBQLN2*^{P497H} (hereafter referred to as *UBQLN2-ALS*) (#83363). The stock line carrying GMR-GAL4 on X chromosome [31] was kindly provided by Yoshida H. (Kyoto Institute of Technology, Kyoto, Japan). Wild-type *Oregon-R* flies were used as reference lineages (Bloomington #2376). To minimize genetic background effects, all experimental flies were backcrossed six times with the *w* strain before use.

Drosophila **life span**

The viability assay was performed as described in [32], with slight modifications. Virgin female flies carrying *nSyb-GAL4* (n = 10) were crossed with male flies carrying *UAS-ERO1L* (n = 10) on either phytochemical-supplemented food or standard medium containing 0.1% DMSO (vehicle control), with three replicates per condition. Phytochemicals were administered at concentrations of 1, 5, or 10 µM. Newly eclosed adult male flies overexpressing *ERO1L* were separated into low-density vials (20 flies per vial) containing either standard medium-vehicle or phytochemical-supplemented food. These flies were maintained under the same temperature and humidity conditions as described earlier. Flies were transferred to fresh food vials every three days, and mortality was recorded. The survival rate was determined as the percentage of surviving flies each day until all flies had died. Comparisons were made between phytochemical-treated and untreated groups. A total of 100 males per group per condition were studied. Survival curves were generated and analyzed using the Log-rank (Mantel-Cox) test for statistical validation.

***Drosophila* locomotive assays**

Virgin female flies carrying *elav-GAL4* (n = 10) were crossed with males carrying *UAS-UBQLN2-ALS* (n = 10) on either standard medium or phytochemical-supplemented food, with three replicates per condition. S88 was provided at 1 or 5 µM, while T2212 was administered at 5 or 10 µM. Third instar larvae were selected for crawling assays, conducted as described in [32]. Larval movement was tracked using ImageJ v1.53K with the wrMTrck plugin, and the distance traveled in 30 seconds was recorded. At least 55 larvae per group per condition were studied. Adult locomotion was assessed using a negative geotaxis assay as described in [33]. Male flies from the same parental cross as described above were sorted and transferred to low-density vials (20 flies per vial) containing either standard medium or phytochemical-supplemented food. S88 was administered at 5 µM, and T2212 was administered at 10 µM. Flies aged 5, 10, 15, 20, 25, and 30 days post-eclosion were gently transferred, without anesthesia, into transparent conical tubes. The flies were acclimated for 10 minutes and then tapped to the bottom every 30 seconds before climbing (10 flies per vial, age-matched). Each trial was recorded and repeated five times. Climbing performance was scored based on the height reached within 5 seconds: 0 (<2.0 cm), 1 (2.0–3.9 cm), 2 (4.0–5.9 cm), 3 (6.0–7.9 cm), 4 (8.0–9.9 cm), and 5 (>10 cm). The climbing index was calculated as the weighted sum of the scores divided by the total number of flies per group. Scores were compared to age-matched controls, with 100 flies analyzed per genotype or treatment unless stated otherwise. Unless otherwise specified, a total of 100 flies per condition were studied.

Neuromuscular junctions' visualization

Third instar larvae expressing UBQLN2-ALS in all neurons (elav-GAL4) were treated with 5 µM S88, 10 µM T2212, or left untreated (vehicle). The larvae were then dissected in haemolymph-like saline (HL3 saline), followed by fixation in 4% paraformaldehyde/PBS for 30 minutes, according to established methods [34]. Blocking was carried out with a PBS solution containing 2% bovine serum albumin (BSA) and

0.1% Triton X-100. For detection, a fluorescein isothiocyanate (FITC)-conjugated goat anti-horseradish peroxidase antibody (1:1000, Jackson ImmunoResearch Laboratories, INC.) was used, and anti-Disc large (Dlg) mouse monoclonal antibody (4F3 anti-discs large, DSHB) was diluted to 1:300. The samples were mounted and examined using a confocal laser-scanning microscope (Olympus Fluoview FV3000). Quantification of glutamatergic motor neuron type I big (Ib) length and bouton counts in muscle 4 of abdominal segment 4 (A4) was performed. Image analysis was done with ImageJ (v. 1.53k). A total of 41, 45, and 40 NMJs from vehicle, S88-treated, and T2212-treated larvae, respectively, were analyzed.

RNA isolation and qPCR

Total RNA was isolated from undifferentiated SH-SY5Y cells using the RNeasy® Mini Kit (QIAGEN) following the manufacturer's protocol. Three biological replicates were performed. RNA purity and concentration were assessed using a NanoDrop One/OneC Spectrophotometer (Thermo Fisher Scientific). Next, 1 µg of total RNA was reverse-transcribed into cDNA with the SensiFAST cDNA Synthesis Kit (Bioline). Quantitative reverse transcription PCR (RT-qPCR) was carried out in triplicate for each RNA sample using the SensiFAST SYBR® Lo-ROX Kit on a CFX Opus Real-Time PCR System (Bio-Rad), with specific primers (Supplementary Table S5). Quantitative normalization for each sample was performed by using *ACTIN* as an internal control.

Proteins isolation and western blotting

Crude extracts were prepared from either third instar foraging larvae (L3) or adult *Drosophila* heads or RA-differentiated SH-SY5Y cells using RIPA Lysis and Extraction Buffer (Thermo Fisher), following the manufacturer's instructions. Briefly, 50 L3 larvae or 40 *Drosophila* heads were homogenized in 400 µl or 100 µl of RIPA buffer supplemented with a protease inhibitor (Thermo Scientific™ Halt™ Protease Inhibitor Cocktail), respectively. SH-SY5Y cells were collected from 6-well plates, washed with PBS, and the cell pellet was resuspended in 60 µl of complete RIPA buffer. The homogenates were incubated at 4°C with gentle rotation for 20 minutes, then centrifuged at 14,000×g at 4°C for 20 minutes. The supernatant (cleared lysate) was collected and protein concentration was determined using the BCA assay kit (Millipore #71285). A total of 30 µg of lysate was loaded onto a 12% polyacrylamide gel and transferred to an Immobilon-P PVDF membrane (Merck) using the Transblot-Turbo transfer system (Bio-Rad). The membranes were blocked with 5% skim milk in TBS-T (Tris-buffered saline with 0.1% Tween® 20) at room temperature and incubated overnight with primary antibodies (listed in Supplementary Table S6). After washing the membranes four times with TBS-T, they were incubated with HRP-conjugated secondary antibodies (1:3000) for 1 hour (Goat Anti-Rabbit or Anti-Mouse IgG (H + L)-HRP Conjugate, Bio-Rad #1706515 and #1706516, respectively). Primary and secondary antibodies were diluted in 5% skim milk in TBS-T. Membranes were developed using WesternSure Chemiluminescent Reagents (LI-COR) and imaged with the C-DiGit Blot Scanner (LI-COR). Protein levels were normalized to housekeeping proteins such as cytoplasmic Actin and nuclear Lamin C. For pEIF2α quantification, samples were normalized to total eIF2α protein levels. Band intensities were quantified using ImageJ software (version 1.53k) across multiple biological replicates.

Data analysis

Statistical analyses were conducted using GraphPad Prism 9 (GraphPad Software). For normally distributed data, comparisons between two groups were made using either the Student's t-test or Welch's t-test, while one-way ANOVA followed by Tukey's or Dunnett's test was applied for comparisons among multiple groups. For data that were not normally distributed, the Mann-Whitney U test was used for two-group comparisons, and Kruskal-Wallis test followed by Dunn's test was used for multiple-group comparisons. Statistical significance was defined as $p < 0.05$. Data are presented as mean ± standard deviation (SD) for experiments with fewer than six replicates, such as Western blots and quantitative PCR. For larger datasets, including neurobehavioral analyses, data are expressed as mean ± standard error of the mean (SEM).

Results

Phytochemical virtual screening identified five potential probe inhibitors specific to ERO1A.

A virtual screening of 401,824 phytochemical compounds was conducted to identify potential ERO1A inhibitors aimed at attenuating the ER stress response (Figure 1). Drug-likeness criteria were applied as an initial filter, excluding a large number of compounds and reducing the dataset to 122,441 candidates (30%).

Next, these compounds were screened for their binding affinity to ERO1A, retaining only those with stronger affinity than EN460 (-8.6 kcal/mol), a known ERO1A inhibitor. This step narrowed the selection to 6,825 compounds (6%).

To ensure specificity for ERO1A, we compared the binding affinities of these compounds against other FAD-containing enzymes, given the highly conserved nature of FAD-binding sites. First, binding affinity to ERO1B, the paralog of ERO1A, was assessed. Only 722 compounds (~11%) exhibited higher affinity for ERO1A than for ERO1B.

These compounds were then further screened against additional FAD-containing enzymes, including MAO-A, MAO-B, and LSD1. The binding energies of these enzymes' known inhibitors—Harmine (-8.7 kcal/mol) for MAO-A, Safinamide (-9.3 kcal/mol) for MAO-B, and CC-90011 (-9.9 kcal/mol) for LSD1—were used as cutoffs for favorable binding. The majority of the compounds exhibited equal or stronger binding to these enzymes than their respective inhibitors, leaving only 18 compounds (3%) that were selective for ERO1A (Supplementary Tables 1-3). Of these 18 compounds, only 8 were available for synthesis, with 5 commercially purchasable at ≥90% purity (Supplementary Table 4). Compounds CNP0392367 and CNP0168092 (hereafter referred to as S43 and S47, respectively) and geniposide were purchasable with a perfect match, while CNP0079545 and CNP0410364 (hereafter referred to as S76 and S88, respectively) were available only as isomers (Supplementary Table 4).

Selected phytochemicals serve as effective ERO1A inhibitors with minimal to negligible cytotoxicity

To experimentally validate the predicted inhibitory activity of selected phytochemicals against ERO1A, we performed an *in vitro* enzymatic assay based on the Amplex®

UltraRed (AUR) system. In this assay, ERO1A, in complex with its redox partner PDI, generates hydrogen peroxide (H_2O_2), which in turn is converted by horseradish peroxidase (HRP) into the fluorescent product resorufin (Figure 2A). The resulting fluorescence intensity serves as a direct readout of ERO1A enzymatic activity and has proven effective for screening and validating novel ERO1A inhibitors. [14,20]. Compared to the uninhibited control, all tested phytochemicals reduced fluorescence intensity, indicating suppression of ERO1A activity (Figure 2B,C). Notably, the extent of inhibition was comparable to that observed with the established ERO1A inhibitor EN460. Among the compounds tested, S47 showed the most pronounced inhibitory effect, consistent with *in silico* predictions (Supplementary Table S3). These findings confirm that the selected phytochemicals directly inhibit ERO1A enzymatic activity *in vitro* and support their potential as functional ERO1A modulators in cellular systems.

To assess the *in vivo* potential of the identified phytochemicals in inhibiting ERO1, we utilized the shortened lifespan of *nSyb>ERO1L* flies, which results from elevated ERO1L (*Drosophila* ortholog of mammalian ERO1A) expression in neurons [11], as a readout. Survival analysis was performed on these flies, both with and without phytochemical treatment, to determine whether the compounds could rescue the lifespan defect, thereby providing further evidence of their ERO1L inhibitory activity. Remarkably, all five identified phytochemicals significantly counteracted the toxicity high ERO1L levels, as demonstrated by the overall increase in median survival compared to untreated flies (Figure 3 A-E). These findings strongly support the hypothesis that these phytochemicals retain the ability to inhibit ERO1L *in vivo*, similarly to EN460 treatment (Figure 3 F, Supplementary Figure S1). However, the flies' responses to the phytochemicals varied depending on the dose and type of compound tested.

S43 and S88 were the most effective in extending lifespan, with 75% of the flies surviving at 60 and 50 days post-eclosion at 5 μM, respectively (Figure 3 A and D). Notably, a 5 μM dose of S43 showed the most pronounced benefit, as the survival probability slope dramatically decreased compared to untreated or other doses, suggesting a potential time-dependent pro-longevity effect that may complement its ERO1L inhibitory activity (Figure 3 A). On the other hand, S47 showed the greatest benefit at the lowest concentration (1 μM), implying potential toxicity related to its metabolism at higher concentrations (Figure 3 B).

Both S76 and T2212 extended lifespan to a lesser degree (Figure 3C and E). S76 demonstrated similar effects at 1, 5, or 10 µM, with a slightly higher impact at 5 µM (Figure 3C). T2212 was most effective at 10 µM (Figure 2E). Finally, S88 consistently extended lifespan across all tested doses, showing the greatest benefits at early life stages, as evidenced by a 25% mortality rate that was higher than that of untreated flies and other phytochemicals. S88 exhibited particularly strong effects at both 1 and 5 µM (Figure 3D).

Next, we investigated the potential cytotoxicity of the identified phytochemicals in human cells to rule out any harmful effects that could limit their use as chemical probe inhibitors of ERO1A. We assessed the effects on primary human-derived fibroblasts (HDF), Hep2G, and SH-SY5Y cell lines after incubation for 24- (Supplementary Figure S2) or 48-hours (h) (Figure 4) with progressively increasing doses of each phytochemical. S43, S47, and S76 showed cytotoxicity in primary cells at the highest doses after 24h (Supplementary Figure S2 A-C), with S47 exhibiting a time-dependent increase in toxicity in HDF (Figure 4C). In contrast, neither S88 nor T2212 showed toxicity in HDF at any incubation time tested (Figure 4E and F, Supplementary Figure S2D and E). Overall, none of the phytochemicals were toxic to Hep2G and SH-SY5Y at any incubation time (Figure 3 and Supplementary Figure S2).

Together, these results confirm that the selected phytochemicals function as *bona fide* ERO1A inhibitors, effectively reducing enzymatic activity *in vitro* and mitigating ERO1L-induced toxicity *in vivo*. Importantly, S88 and T2212 exhibited minimal to negligible cytotoxicity in multiple human cell types, supporting their suitability for further development. These findings establish a strong foundation for investigating the molecular mechanisms underlying their protective effects and therapeutic potential in ER stress–related pathologies.

S88 and T2212 alleviate ER stress markers and enhance survival in Tm-stressed neuronal cells

Building on our previous findings that pharmacological inhibition of ERO1L with EN460 attenuates the unfolded protein response (UPR) in both tunicamycin-challenged wild-type *Drosophila* and in flies expressing the familial Amyotrophic Lateral Sclerosis (ALS)-associated *UBQLN2*^{P497H} mutation [11], we next investigated whether the identified phytochemicals could similarly modulate ER stress markers. To this end, we initially focused on SH-SY5Y neuroblastoma cells, a relevant model given the involvement of ERO1A signaling in neurodegenerative processes.

We first established an optimized model for ER stress induction by treating undifferentiated SH-SY5Y cells with 1 μM tunicamycin (Tm) and monitored cell viability along with the expression of key ER stress markers over time (Supplementary Figure S3A). As expected, Tm exhibited a time-dependent cytotoxic effect, with a significant reduction in cell viability after 48h (Supplementary Figure S3 B-D). Interestingly, ER stress markers peaked at 24h before declining, suggesting an early transcriptional response followed by progressive cellular damage (Supplementary Figure S3 E). Based on these findings, we chose a 48h Tm incubation period for subsequent experiments.

To assess the beneficial effects of phytochemicals, we employed a stepwise treatment approach, administering the compounds after the onset of cellular stress. This involved an initial 24h exposure to Tm, followed by a 24h treatment with each phytochemical at either 10 or 20 μM (Figure 5A and Supplementary Figure S4A). Cell viability and ER stress markers were evaluated at the end of the treatment period. Interestingly, among the five tested compounds, only S88 and T2212 consistently improved cell viability under these experimental conditions while significantly reducing all measured ER stress markers (Supplementary Figure S4B, C and Figure 5B). Notably, S76 showed the highest increase in cell viability (Supplementary Figure S4B); however, this effect was not accompanied by a general reduction in ER stress markers. Only *HSPA5* levels were lower compared to the untreated Tm-stressed control when S76 was provided at 20 μM (Figure 5 B). Similarly, S43 improved cell survival but at the same time led to an increase in most ER stress markers, with the exception of *ATF4*, which remained unchanged (Supplementary Figure S4C and Figure 5B).

These findings suggest that the identified phytochemicals may confer protection under ER stress through distinct mechanisms, with only S88 and T2212 consistently enhancing cell survival while reducing ER stress markers. Given our objective of identifying compounds that inhibit ERO1A and alleviate ER stress, we prioritized S88 and T2212 for further investigation.

Next, we validated our findings in mature neurons and sought to determine an appropriate Tm dose that induces ER stress without causing excessive cell death. SH-SY5Y cells were differentiated with RA (Supplementary Figure S5A), and as expected, neurite elongation was accompanied by a progressive increase in key neuronal maturation markers (Supplementary Figure S5B, C). Meanwhile, Tm exhibited a time- and dose-dependent cytotoxic effect, with significant cell death observed after 48h of exposure to 10 μM Tm (Supplementary Figure S6). Based on these findings, we implemented a 24h preconditioning step with 1 μM Tm (Tm-1) in 3-day RA-differentiated SH-SY5Y cells, followed by a 24h intervention with S88 or T2212 in the continued presence of Tm-1 (Figure 5C). Here, both phytochemicals improved neuronal survival under ER stress in a dose-dependent manner, with maximal protection observed at 2.5 μM and a decline in efficacy at higher concentrations (Figure 5D and E).

We next examined canonical markers of ER stress under these experimental conditions and found that treatment with 2.5 μM S88 or T2212 significantly reduced the levels of PERK, BiP, ATF4, and phosphorylated eIF2α (eIF2α-pSer51) compared to Tm-stressed neurons without phytochemical treatment (Figure 5F-J).

Taken together, these results indicate that both S88 and T2212 enhance neuronal survival under Tm-induced ER stress, likely through partial modulation of the UPR signaling pathway. These findings further support their candidacy as neuroprotective agents and prompted us to further investigate the mechanisms of action of S88 and T2212 in a more physiologically relevant context.

S88 and T2212 improve early neuronal health in UBQLN2^{ALS} models, but only S88 preserves locomotor function throughout disease progression

Next, we turned to a *Drosophila* model of neurodegeneration, which offers a complex *in vivo* system recapitulating key features of ER stress-associated neuronal pathology [35-37]. We previously demonstrated that pharmacological inhibition of ERO1L with EN460 can improve pathophysiology of flies expressing the familial ALS-associated UBQLN2^{P497H} variant (UBQLN2^{ALS})[11,38], a model in which chronic ER stress and maladaptive UPR activation are key pathogenic features [39-41]. Notably, this rescue effect is specifically linked to ERO1L suppression, as we further showed that pan-neuronal *ERO1L* knockdown also restores locomotor function in this UBQLN2^{ALS} model (Supplementary Figure S7).

To assess the effects of S88 and T2212, increasing concentrations were administered to the parental cross and maintained throughout the development of the F1 generation (Figure 6A). Locomotor function was evaluated in larvae expressing UBQLN2^{ALS} in all neurons and compared to untreated controls (vehicle, veh). A dose-dependent improvement in locomotion was observed (Figure 6B-C), alongside significant NMJ health benefits, including increased branch length and a higher number of synaptic boutons (Figure 6D-F, Supplementary Figure S8 and S9). Notably, S88 was effective at both 1 µM and 5 µM, whereas T2212 showed benefits only at the higher dose of 10 µM (Figure 6B-F).

To determine whether these improvements persisted into adulthood, we assessed locomotor performance in adult flies at different time points during aging (Figure 6G). Climbing assays revealed that only S88 treatment resulted in a sustained enhancement of motor function, with treated flies exhibiting significantly better climbing ability compared to vehicle-treated controls. This effect was evident in young flies (5-day old, D5) and persisted through the late stages of the disease (30-day old, D30). In contrast, T2212-treated flies did not maintain improved motor performance beyond the larval stage, as their climbing ability declined similarly to untreated flies over time (Figure 6G). These findings suggest that while both compounds provide early benefits, only S88 confers long-term neuroprotection, preserving locomotor function throughout disease progression.

To determine whether the locomotor improvements observed in UBQLN2^{ALS} *Drosophila* models following phytochemical treatment were associated with ER stress modulation, we analyzed UPR markers and stress-responsive gene expression across disease stages and tissues (Figure 7A, Supplementary Figure S10A). Immunoblot analysis revealed that both S88 and T2212 reduced phosphorylated eIF2α (eIF2α-pSer51) at larval and adult stages (D30), indicative of attenuated ER stress (Figure 7B, D, F, H). However, ATF4 (Crc in *Drosophila*) protein levels remained unchanged in S88-treated flies, despite reduced p-eIF2α (Figure 7C, G), suggesting an alternative mechanism sustaining ATF4 expression. Given reports of p-eIF2α–independent ATF4 regulation via mTORC1 and 4E-BP1 [42,43], we assessed mTORC1 activation by probing p70S6K and 4E-BP1 phosphorylation. Neither showed changes upon S88 treatment at any time point (Supplementary Figure S10), arguing against mTORC1 involvement.

Transcriptional profiling uncovered distinct tissue- and stage-specific responses. In fly heads, both phytochemicals reduced multiple ER stress and cytoprotective gene transcripts at day 15 (D15-H), but this response waned by day 30 (D30-H), except for sustained *Sip3* downregulation in S88-treated flies (Supplementary Figure S11B, D). In the body (carcass, C), a more heterogeneous response emerged: *ATF4* mRNA was downregulated at D15 but trended upward at D30, while *ATF6* was consistently suppressed across treatments and time points. Additional markers such as *Pdi*, *Erp60*, *Hsp22*, and *Sip3* exhibited dynamic or compound-specific regulation, with S88 producing a more consistent downregulation of Sip3 and Hsp22 (Supplementary Figure S11C, E).

Together, these data suggest that both S88 and T2212 mitigate ER stress during early disease. However, only S88 induces a residual stress-adaptive transcriptional program that persists into late-stage neurodegeneration, coupled with sustained ATF4 protein levels via a mechanism independent of both eIF2α phosphorylation and mTORC1.

S88 counters accelerated aging in a D-Galactose *Drosophila* Model

Aging is marked by a progressive loss of proteostasis and heightened vulnerability to ER stress [4,44,45], processes in which ERO1A plays a central role [46,47]. Building on the neuroprotective effects of S88 and T2212 under both environmental (Tm-induced) and genetic (UBQLN2^{ALS}-driven) ER stress, we next evaluated their therapeutic potential in a model of organismal aging. To this end, we employed a *Drosophila* model of accelerated aging induced by chronic D-galactose (D-GAL) exposure, which recapitulates key features of aging, including oxidative stress, mitochondrial dysfunction, and reduced lifespan [48,49]. This system provides a platform to assess whether pharmacological inhibition of ERO1A can mitigate aging-associated decline and improve survival. Following dose-dependent evaluation (Supplementary Figure S12), 25 mM D-GAL was chosen for subsequent experiments as it induces a robust but not overly severe aging phenotype, allowing greater sensitivity to detect protective effects.

Pharmacological treatment with S88 significantly extended lifespan at both 1 µM and 5 µM doses (S88-1 and S88-5), compared to untreated controls (Figure 8A). In contrast, T2212 failed to confer any survival benefit at either 5 µM or 10 µM, indicating a lack of efficacy in this aging context (Figure 8B). These findings suggest that S88 retains protective effects in aging-related decline, whereas T2212 does not impact organismal survival under chronic oxidative and proteotoxic stress.

Discussion

Maladaptive ER stress responses are increasingly recognized as key contributors to the pathogenesis of neurodegenerative and age-associated disorders [50-52]. ERO1A, an oxidoreductase that drives oxidative protein folding in the ER, plays a central role in amplifying ER stress and is thus an attractive but underexplored therapeutic target [53,54]. Despite this, selective and non-toxic inhibitors of ERO1A remain scarce. Here, we employed a structure-based virtual screening strategy combined with multi-tiered functional validation to identify five novel phytochemical inhibitors of ERO1A. Among them, S88 and T2212 emerged as lead candidates with favorable specificity, bioactivity, and safety profiles.

A stringent computational pipeline was used to identify compounds with preferential binding to ERO1A over other FAD-dependent enzymes, including its paralog ERO1B. This led to the selection of five commercially available phytochemicals, all of which reduced ERO1A enzymatic activity *in vitro* to levels comparable with the reference inhibitor EN460. *In vivo*, all five compounds improved survival in flies overexpressing neuronal ERO1L, the *Drosophila* ortholog of ERO1A, with S88 and S43 showing the strongest protective effects. While the observed rescue of ERO1L-induced toxicity in *Drosophila* supports ERO1A as the relevant *in vivo* target, further studies will be required to fully exclude potential off-target effects, especially in mammalian systems.

Among the selected phytochemicals, T2212 (also known as geniposide) has previously been reported to possess neuroprotective properties and to modulate ER stress [55,56]. However, its mechanism of action had not been linked to ERO1A inhibition prior to this study. In contrast, S88 represents a novel ERO1A-targeting compound with no prior association to ER stress modulation. In human cell models of ER stress, both S88 and T2212 significantly enhanced cell survival while reducing canonical UPR markers, including BiP, PERK, ATF4, and phosphorylated eIF2α. These effects were preserved in differentiated SH-SY5Y neurons, highlighting their therapeutic relevance in a neuronal context. Notably, S88 was effective at lower doses and exhibited minimal cytotoxicity across multiple human cell lines, underscoring its favorable safety profile.

Interestingly, although S43, S47, and S76 improved neuronal survival under Tm-induced ER stress, they did not significantly reduce ER stress markers *in vitro*. This divergence is notable, as both genetic and pharmacological inhibition of ERO1L, *via* RNAi or the known inhibitor EN460, consistently leads to downregulation of UPR markers [11]. Given that S43, S47, and S76 inhibit ERO1A *in vitro* and extend lifespan in flies overexpressing neuronal ERO1L, one would expect them to also alleviate ER stress in neuronal cells. However, their lack of effect on UPR markers suggests that additional factors may limit their activity in this context. One possible explanation is that differences in cell permeability or intracellular stability may prevent these compounds from reaching sufficient concentrations in stressed neurons to inhibit ERO1A effectively. Alternatively, the environment of acute ER stress, induced pharmacologically by Tm, may alter the accessibility or redox compatibility of ERO1A, limiting compound engagement. In contrast, S88 and T2212 appear to retain sufficient stability and target access to effectively engage ERO1A under stress conditions.

Importantly, despite their inability to suppress ER stress markers, S43, S47, and S76 still improved survival in both *Drosophila* overexpressing ERO1L and Tm-stressed neurons. This suggests that their protective effects may arise through mechanisms independent of direct ERO1A inhibition, such as modulation of oxidative stress, mitochondrial support, or general stress resilience pathways.

As chronic ER stress is a central feature of neurodegenerative and age-related diseases, our screening strategy specifically aimed to identify compounds that can directly attenuate ER stress signaling. These findings emphasize the importance of combining cell viability assays with mechanistic readouts to distinguish non-specific cytoprotection from genuine pathway modulation. In this context, the ability of S88 and T2212 to both improve neuronal survival and consistently reduce UPR markers supports the use of ER stress attenuation as a biologically meaningful and mechanistically stringent criterion for advancing candidate ER stress-modulating compounds. Finally, we prioritized S88 and T2212 for further development, as their consistent efficacy in reducing UPR markers in stressed human neurons represents a more stringent and translationally relevant criterion for advancing candidate therapeutics targeting ER stress-related disorders.

The neuroprotective potential of S88 and T2212 was further confirmed in a *Drosophila* model of ALS expressing the pathogenic UBQLN2^{P497H} mutation, a context in which chronic ER stress and dysregulated UPR signaling are known pathogenic drivers [40,57,58]. Both compounds improved early motor performance and neuromuscular junction integrity, but only S88 conferred lasting benefits throughout disease progression. This persistent rescue was associated with continued suppression of ER stress markers and selective transcriptional adaptations in late-stage brains. Interestingly, ATF4 protein levels remained elevated in S88-treated flies despite reduced eIF2α phosphorylation and unaltered mTORC1 activity, suggesting an alternative, possibly stress-adaptive mode of ATF4 regulation that may contribute to S88's sustained efficacy and warrants deeper mechanistic exploration.

We further demonstrated that S88, but not T2212, significantly extended lifespan in a D-GAL–induced *Drosophila* model of accelerated aging. Although many natural compounds exert anti-aging effects through antioxidant properties [59-61], radical scavenging assays (DPPH and ABTS) confirmed that neither S88 nor T2212 possess substantial antioxidant activity. This supports the notion that ERO1A inhibition, rather than general redox buffering, likely underlies their protective effects.

The observation that genetic knockdown of *ERO1A* can ameliorate *UBQLN2*^{ALS}-associated phenotypes in late-stage disease and extend lifespan in aging flies suggests that the magnitude and durability of ERO1A inhibition are critical determinants of therapeutic benefit. Although T2212 effectively attenuated ER stress markers and improved early neuronal outcomes, it failed to confer benefits in late-stage ALS or aging models. One plausible explanation is that T2212 may have suboptimal metabolic stability or biodistribution, potentially leading to reduced efficacy or time-dependent accumulation of bioactive metabolites with off-target or toxic effects that mask its initial therapeutic activity.

In contrast, S88 maintained efficacy across models and disease stages. Structurally, S88 is a pyrazolopyridine-based heterocyclic alkaloid, a scaffold of growing interest in medicinal chemistry [62]. Pyrazolopyridines are a versatile class of chemical compounds that combine the biologically privileged pyrazole and pyridine rings, both recognized for their broad spectrum of bioactivities such as anti-inflammatory, antioxidant, anticancer, and neuroprotective effects [63,64]. This unique fused scaffold frequently acts as modulators of various enzyme targets and receptor systems, contributing to their diverse pharmacological profiles. Notably, pyrazolopyridines can function as allosteric modulators of GABA receptors, inhibitors of enzymes including thrombin and orotidine 5'-monophosphate decarboxylase, and ligands for G-protein coupled receptors (GPCRs) [65,66]. In recent years, several FDA-approved drugs incorporating a pyrazolone core have been investigated for therapeutic use. Notably, edaravone, which features this scaffold, has been utilized as a free radical scavenger in the treatment of amyotrophic lateral sclerosis (ALS) [67].

Taken together, our findings establish S88 as a novel ERO1A inhibitor with robust neuroprotective and anti-aging properties. Future studies aimed at elucidating the downstream regulatory networks of ERO1A inhibition and refining the pharmacological profile of S88 may pave the way for the development of novel therapies for ER stress-associated disorders.

Conclusion

Our findings demonstrate that targeting ERO1A with novel natural small chemicla inhibitors can effectively alleviate neuronal ER stress and improve aging. S88 emerges as a particularly promising candidate, displaying sustained benefits in neuromuscular function and lifespan extension. This study highlights the power of a multi-modal drug discovery approach in identifying selective ERO1A inhibitors and lays the foundation for further therapeutic development of S88 for ER stress-related diseases.

CRediT authorship contribution statement

Conceptualization: S.J. and L.LP; Data curation: S.J., A.S. and L.LP; Formal Analysis: S.J, A.S., N.U and L.LP.; Funding acquisition; L.LP; Investigation: S.J., A.S., U.N., W.W, P.P, R.Y., and L.LP; Methodology: S.J., A.S. and L.LP; Project administration: L.LP; Resources; L.LP and S.J; Software: A.S. and L.LP.; Supervision; L.LP; Validation: S.J., A.S. and L.LP.; Visualization: A.S. and L.LP; Writing – original draft: S.J., A.S. and L.LP.; Writing – review & editing: All authors have reviewed and approved the final version of this manuscript.

Declaration of competing interest

The authors declare that they have no known competing financial interests or personal relationships that could have appeared to influence the work reported in this paper.

Acknowledgements

We would like to express our gratitude to the administrative office and technical staff of CMUTEAM, as well as the staff of the Department of Pharmacology, Faculty of Medicine, Chiang Mai University, for their generous support. In particular, we acknowledge Ms Thunpitcha Meesawat for administrative assistance and sincerely thank Mr. Papon Hitmool, Mr. Sakorn Phongchankhiao, Ms Ratchanaree Suepsaipaeng, Ms Chansunee Panto and Mr. Tawan Munwanna for technical assistance. We are also grateful to Yoshida Hideki (Kyoto Institute of Technology) and the Bloomington Stock Center for providing fly strains, the Science and Educational

Company Limited (SCIED) for training in confocal scanning electron microscopy. Finally, we sincerely appreciate Dr. Natrujee Wiwattanadittakul, M.D. (Faculty of Medicine, Chiang Mai University), for collecting skin specimens for fibroblast isolation and extend our gratitude to the anonymous donor for the participation in this study.

Funding

This study was supported by Fundamental Fund, Chiang Mai University under the grants FF67/044 and FF66/061 and supported by the Faculty of Medicine, Chiang Mai University grant no FACMED 139/2567. This study was partially supported by Genomics Thailand, Health Systems Research Institute (HSRI) under grants 66-124 and 68-060.

Data Availability

The authors confirm that the data supporting the findings of this study are available within the article and its supplementary material.

References

1 Lindholm, D., Wootz, H. & Korhonen, L. ER stress and neurodegenerative diseases. *Cell Death Differ* **13**, 385-392 (2006). https://doi.org:10.1038/sj.cdd.4401778

2 Sprenkle, N. T., Sims, S. G., Sanchez, C. L. & Meares, G. P. Endoplasmic reticulum stress and inflammation in the central nervous system. *Mol Neurodegener* **12**, 42 (2017). https://doi.org:10.1186/s13024-017-0183-y

3 Xiang, C., Wang, Y., Zhang, H. & Han, F. The role of endoplasmic reticulum stress in neurodegenerative disease. *Apoptosis* **22**, 1-26 (2017). https://doi.org:10.1007/s10495-016-1296-4

4 Chen, X., Shi, C., He, M., Xiong, S. & Xia, X. Endoplasmic reticulum stress: molecular mechanism and therapeutic targets. *Signal Transduct Target Ther* **8**, 352 (2023). https://doi.org:10.1038/s41392-023-01570-w

5 Pollard, M. G., Travers, K. J. & Weissman, J. S. Ero1p: a novel and ubiquitous protein with an essential role in oxidative protein folding in the endoplasmic reticulum. *Mol Cell* **1**, 171-182 (1998). https://doi.org:10.1016/s1097-2765(00)80018-0

6 Zhang, J. *et al.* Endoplasmic Reticulum stress-dependent expression of ERO1L promotes aerobic glycolysis in Pancreatic Cancer. *Theranostics* **10**, 8400-8414 (2020). https://doi.org:10.7150/thno.45124

7 Bassot, A. *et al.* The endoplasmic reticulum kinase PERK interacts with the oxidoreductase ERO1 to metabolically adapt mitochondria. *Cell Rep* **42**, 111899 (2023). https://doi.org:10.1016/j.celrep.2022.111899

8 Haynes, C. M., Titus, E. A. & Cooper, A. A. Degradation of misfolded proteins prevents ER-derived oxidative stress and cell death. *Mol Cell* **15**, 767-776 (2004). https://doi.org:10.1016/j.molcel.2004.08.025

9 Marciniak, S. J. *et al.* CHOP induces death by promoting protein synthesis and oxidation in the stressed endoplasmic reticulum. *Genes Dev* **18**, 3066-3077 (2004). https://doi.org:10.1101/gad.1250704

10 Curran, S. P. & Ruvkun, G. Lifespan regulation by evolutionarily conserved genes essential for viability. *PLoS Genet* **3**, e56 (2007). https://doi.org:10.1371/journal.pgen.0030056

11 Yeewa, R. *et al.* ERO1A inhibition mitigates neuronal ER stress and ameliorates UBQLN2(ALS) phenotypes in Drosophila melanogaster. *Prog Neurobiol* **242**, 102674 (2024). https://doi.org:10.1016/j.pneurobio.2024.102674

12 Pagani, M. *et al.* Endoplasmic reticulum oxidoreductin 1-lbeta (ERO1-Lbeta), a human gene induced in the course of the unfolded protein response. *J Biol Chem* **275**, 23685-23692 (2000). https://doi.org:10.1074/jbc.M003061200

13 Zito, E., Chin, K. T., Blais, J., Harding, H. P. & Ron, D. ERO1-beta, a pancreas-specific disulfide oxidase, promotes insulin biogenesis and glucose homeostasis. *J Cell Biol* **188**, 821-832 (2010). https://doi.org:10.1083/jcb.200911086

14 Blais, J. D. *et al.* A small molecule inhibitor of endoplasmic reticulum oxidation 1 (ERO1) with selectively reversible thiol reactivity. *J Biol Chem* **285**, 20993-21003 (2010). https://doi.org:10.1074/jbc.M110.126599

15 Voronkova, M. A. *et al.* ERO1A levels are a prognostic indicator in EGFR mutated non small cell lung cancer. *NPJ Precis Oncol* **8**, 250 (2024). https://doi.org:10.1038/s41698-024-00736-1

16 Salvagno, C., Mandula, J. K., Rodriguez, P. C. & Cubillos-Ruiz, J. R. Decoding endoplasmic reticulum stress signals in cancer cells and antitumor immunity. *Trends Cancer* **8**, 930-943 (2022). https://doi.org:10.1016/j.trecan.2022.06.006

17 Marciniak, S. J., Chambers, J. E. & Ron, D. Pharmacological targeting of endoplasmic reticulum stress in disease. *Nat Rev Drug Discov* **21**, 115-140 (2022). https://doi.org:10.1038/s41573-021-00320-3

18 Germani, S. *et al.* SEPN1-related myopathy depends on the oxidoreductase ERO1A and is druggable with the chemical chaperone TUDCA. *Cell Rep Med* **5**, 101439 (2024). https://doi.org:10.1016/j.xcrm.2024.101439

19 Hayes, K. E. *et al.* Inhibition of the FAD containing ER oxidoreductin 1 (Ero1) protein by EN-460 as a strategy for treatment of multiple myeloma. *Bioorg Med Chem* **27**, 1479-1488 (2019). https://doi.org:10.1016/j.bmc.2019.02.016

20 Johnson, B. D. *et al.* Identification of Natural Product Sulfuretin Derivatives as Inhibitors for the Endoplasmic Reticulum Redox Protein ERO1alpha. *ACS Bio Med Chem Au* **2**, 161-170 (2022). https://doi.org:10.1021/acsbiomedchemau.1c00062

21 Varone, E. *et al.* Small molecule-mediated inhibition of the oxidoreductase ERO1A restrains aggressive breast cancer by impairing VEGF and PD-L1 in the tumor microenvironment. *Cell Death Dis* **16**, 105 (2025). https://doi.org:10.1038/s41419-025-07426-1

22 Atanasov, A. G., Zotchev, S. B., Dirsch, V. M., International Natural Product Sciences, T. & Supuran, C. T. Natural products in drug discovery: advances and opportunities. *Nat Rev Drug Discov* **20**, 200-216 (2021). https://doi.org:10.1038/s41573-020-00114-z

23 Xie, S., Zhan, F., Zhu, J., Xu, S. & Xu, J. The latest advances with natural products in drug discovery and opportunities for the future: a 2025 update. *Expert Opin Drug Discov* **20**, 827-843 (2025). https://doi.org:10.1080/17460441.2025.2507382

24 Waterhouse, A. *et al.* SWISS-MODEL: homology modelling of protein structures and complexes. *Nucleic Acids Res* **46**, W296-W303 (2018). https://doi.org:10.1093/nar/gky427

25 Ropp, P. J. *et al.* Gypsum-DL: an open-source program for preparing small-molecule libraries for structure-based virtual screening. *J Cheminform* **11**, 34 (2019). https://doi.org:10.1186/s13321-019-0358-3

26 Morris, G. M. *et al.* AutoDock4 and AutoDockTools4: Automated docking with selective receptor flexibility. *J Comput Chem* **30**, 2785-2791 (2009). https://doi.org:10.1002/jcc.21256

27 Trott, O. & Olson, A. J. AutoDock Vina: improving the speed and accuracy of docking with a new scoring function, efficient optimization, and multithreading. *J Comput Chem* **31**, 455-461 (2010). https://doi.org:10.1002/jcc.21334

28 Kiriya, C., Yeewa, R., Khanaree, C. & Chewonarin, T. Purple rice extract inhibits testosterone-induced rat prostatic hyperplasia and growth of human prostate cancer cell line by reduction of androgen receptor activation. *J Food Biochem* **43**, e12987 (2019). https://doi.org:10.1111/jfbc.12987

29 Re, R. *et al.* Antioxidant activity applying an improved ABTS radical cation decolorization assay. *Free Radic Biol Med* **26**, 1231-1237 (1999). https://doi.org:10.1016/s0891-5849(98)00315-3

30 Brand, A. H. & Perrimon, N. Targeted gene expression as a means of altering cell fates and generating dominant phenotypes. *Development* **118**, 401-415 (1993). https://doi.org:10.1242/dev.118.2.401

31 Takahashi, Y., Hirose, F., Matsukage, A. & Yamaguchi, M. Identification of three conserved regions in the DREF transcription factors from Drosophila melanogaster and Drosophila virilis. *Nucleic Acids Res* **27**, 510-516 (1999). https://doi.org:10.1093/nar/27.2.510

32 Lo Piccolo, L. *et al.* FAME4-associating YEATS2 knockdown impairs dopaminergic synaptic integrity and leads to seizure-like behaviours in Drosophila melanogaster. *Prog Neurobiol* **233**, 102558 (2024). https://doi.org:10.1016/j.pneurobio.2023.102558

33 Jantrapirom, S., Lo Piccolo, L., Yoshida, H. & Yamaguchi, M. Depletion of Ubiquilin induces an augmentation in soluble ubiquitinated Drosophila TDP-43 to drive neurotoxicity in the fly. *Biochim Biophys Acta Mol Basis Dis* **1864**, 3038-3049 (2018). https://doi.org:10.1016/j.bbadis.2018.06.017

34 Lo Piccolo, L. & Yamaguchi, M. RNAi of arcRNA hsromega affects sub-cellular localization of Drosophila FUS to drive neurodiseases. *Exp Neurol* **292**, 125-134 (2017). https://doi.org:10.1016/j.expneurol.2017.03.011

35 Ryoo, H. D. Drosophila as a model for unfolded protein response research. *BMB Rep* **48**, 445-453 (2015). https://doi.org:10.5483/bmbrep.2015.48.8.099

36 Yan, C. *et al.* IRE1 promotes neurodegeneration through autophagy-dependent neuron death in the Drosophila model of Parkinson's disease. *Cell Death Dis* **10**, 800 (2019). https://doi.org:10.1038/s41419-019-2039-6

37 Katsube, H., Hinami, Y., Yamazoe, T. & Inoue, Y. H. Endoplasmic reticulum stress-induced cellular dysfunction and cell death in insulin-producing cells results in diabetes-like phenotypes in Drosophila. *Biol Open* **8** (2019). https://doi.org:10.1242/bio.046524

38 Deng, H. X. *et al.* Mutations in UBQLN2 cause dominant X-linked juvenile and adult-onset ALS and ALS/dementia. *Nature* **477**, 211-215 (2011). https://doi.org:10.1038/nature10353

39 Wu, J. J. *et al.* ALS/FTD mutations in UBQLN2 impede autophagy by reducing autophagosome acidification through loss of function. *Proc Natl Acad Sci U S A* **117**, 15230-15241 (2020). https://doi.org:10.1073/pnas.1917371117

40 Halloran, M. *et al.* Amyotrophic lateral sclerosis-linked UBQLN2 mutants inhibit endoplasmic reticulum to Golgi transport, leading to Golgi fragmentation and ER stress. *Cell Mol Life Sci* **77**, 3859-3873 (2020). https://doi.org:10.1007/s00018-019-03394-w

41 Renaud, L., Picher-Martel, V., Codron, P. & Julien, J. P. Key role of UBQLN2 in pathogenesis of amyotrophic lateral sclerosis and frontotemporal dementia. *Acta Neuropathol Commun* **7**, 103 (2019). https://doi.org:10.1186/s40478-019-0758-7

42 Torrence, M. E. *et al.* The mTORC1-mediated activation of ATF4 promotes protein and glutathione synthesis downstream of growth signals. *Elife* **10** (2021). https://doi.org:10.7554/eLife.63326

43 Ben-Sahra, I., Hoxhaj, G., Ricoult, S. J. H., Asara, J. M. & Manning, B. D. mTORC1 induces purine synthesis through control of the mitochondrial tetrahydrofolate cycle. *Science* **351**, 728-733 (2016). https://doi.org:10.1126/science.aad0489

44 Hetz, C. & Dillin, A. Central role of the ER proteostasis network in healthy aging. *Trends Cell Biol* (2024). https://doi.org:10.1016/j.tcb.2024.10.003

45 Lopez-Otin, C., Blasco, M. A., Partridge, L., Serrano, M. & Kroemer, G. The hallmarks of aging. *Cell* **153**, 1194-1217 (2013). https://doi.org:10.1016/j.cell.2013.05.039

46 Bhattarai, K. R., Riaz, T. A., Kim, H. R. & Chae, H. J. The aftermath of the interplay between the endoplasmic reticulum stress response and redox signaling. *Exp Mol Med* **53**, 151-167 (2021). https://doi.org:10.1038/s12276-021-00560-8

47 Qiao, X. *et al.* ER reductive stress caused by Ero1alpha S-nitrosation accelerates senescence. *Free Radic Biol Med* **180**, 165-178 (2022). https://doi.org:10.1016/j.freeradbiomed.2022.01.006

48 Azman, K. F. & Zakaria, R. D-Galactose-induced accelerated aging model: an overview. *Biogerontology* **20**, 763-782 (2019). https://doi.org:10.1007/s10522-019-09837-y

49 Shwe, T., Pratchayasakul, W., Chattipakorn, N. & Chattipakorn, S. C. Role of D-galactose-induced brain aging and its potential used for therapeutic interventions. *Exp Gerontol* **101**, 13-36 (2018). https://doi.org:10.1016/j.exger.2017.10.029

50 Ajoolabady, A., Lindholm, D., Ren, J. & Pratico, D. ER stress and UPR in Alzheimer's disease: mechanisms, pathogenesis, treatments. *Cell Death Dis* **13**, 706 (2022). https://doi.org:10.1038/s41419-022-05153-5

51 Meares, G. P. *et al.* PERK-dependent activation of JAK1 and STAT3 contributes to endoplasmic reticulum stress-induced inflammation. *Mol Cell Biol* **34**, 3911-3925 (2014). https://doi.org:10.1128/MCB.00980-14

52 Bellani, S. *et al.* GRP78 clustering at the cell surface of neurons transduces the action of exogenous alpha-synuclein. *Cell Death Differ* **21**, 1971-1983 (2014). https://doi.org:10.1038/cdd.2014.111

53 Shergalis, A. G., Hu, S., Bankhead, A., 3rd & Neamati, N. Role of the ERO1-PDI interaction in oxidative protein folding and disease. *Pharmacol Ther* **210**, 107525 (2020). https://doi.org:10.1016/j.pharmthera.2020.107525

54 Jha, V. *et al.* ERO1-PDI Redox Signaling in Health and Disease. *Antioxid Redox Signal* **35**, 1093-1115 (2021). https://doi.org:10.1089/ars.2021.0018

55 Yamazaki, M., Chiba, K. & Yoshikawa, C. Genipin suppresses A23187-induced cytotoxicity in neuro2a cells. *Biol Pharm Bull* **32**, 1043-1046 (2009). https://doi.org:10.1248/bpb.32.1043

56 Ma, Z. G. *et al.* Protection against cardiac hypertrophy by geniposide involves the GLP-1 receptor / AMPKalpha signalling pathway. *Br J Pharmacol* **173**, 1502-1516 (2016). https://doi.org:10.1111/bph.13449

57 Peng, G. *et al.* Amyotrophic lateral sclerosis (ALS) linked mutation in Ubiquilin 2 affects stress granule assembly via TIA-1. *CNS Neurosci Ther* **28**, 105-115 (2022). https://doi.org:10.1111/cns.13757

58 Le, N. T. *et al.* Motor neuron disease, TDP-43 pathology, and memory deficits in mice expressing ALS-FTD-linked UBQLN2 mutations. *Proc Natl Acad Sci U S A* **113**, E7580-E7589 (2016). https://doi.org:10.1073/pnas.1608432113

59 Chen, Y. *et al.* Dietary Supplements and Natural Products: An Update on Their Clinical Effectiveness and Molecular Mechanisms of Action During Accelerated Biological Aging. *Front Genet* **13**, 880421 (2022). https://doi.org:10.3389/fgene.2022.880421

60 Xu, D. P. *et al.* Natural Antioxidants in Foods and Medicinal Plants: Extraction, Assessment and Resources. *Int J Mol Sci* **18** (2017). https://doi.org:10.3390/ijms18010096

61 Forni, C. *et al.* Beneficial Role of Phytochemicals on Oxidative Stress and Age-Related Diseases. *Biomed Res Int* **2019**, 8748253 (2019). https://doi.org:10.1155/2019/8748253

62 Zhao, Z. *et al.* Pyrazolone structural motif in medicinal chemistry: Retrospect and prospect. *Eur J Med Chem* **186**, 111893 (2020). https://doi.org:10.1016/j.ejmech.2019.111893

63 Atukuri, D. Pyrazolopyridine: An efficient pharmacophore in recent drug design and development. *Chem Biol Drug Des* **100**, 376-388 (2022). https://doi.org:10.1111/cbdd.14098

64 Waly, O. M., El-Sayed, S. M., Ghaly, M. A. & El-Subbagh, H. I. Multi-targeted anti-Alzheimer's agents: Synthesis, biological evaluation, and molecular modeling study of some pyrazolopyridine hybrids. *Eur J Med Chem* **262**, 115880 (2023). https://doi.org:10.1016/j.ejmech.2023.115880

65 Varagic, Z. *et al.* Identification of novel positive allosteric modulators and null modulators at the GABAA receptor alpha+beta- interface. *Br J Pharmacol* **169**, 371-383 (2013). https://doi.org:10.1111/bph.12151

66 Bussel, J. B. *et al.* Eltrombopag for the treatment of chronic idiopathic thrombocytopenic purpura. *N Engl J Med* **357**, 2237-2247 (2007). https://doi.org:10.1056/NEJMoa073275

67 Lapchak, P. A. A critical assessment of edaravone acute ischemic stroke efficacy trials: is edaravone an effective neuroprotective therapy? *Expert Opin Pharmacother* **11**, 1753-1763 (2010). https://doi.org:10.1517/14656566.2010.493558

Figure Legends

Figure 1 The workflow of the docking-based virtual screening process of phytochemical compounds targeting ERO1A. A) The 3D structure of human ERO1A (PDB ID 3AHQ) was prepared with a grid box defined around the binding pocket for docking simulations. Phytochemical compounds from the COCONUT database underwent virtual screening, starting with drug-likeness filtering. The remaining compounds were predicted in 3D and docked to ERO1A to assess binding affinities. Only compounds with a binding affinity higher than EN460, a known ERO1A inhibitor, were selected. Sequential docking against other FAD-containing enzymes (ERO1B, MAO-A, MAO-B, and LSD1) ensured specificity with only compounds showing minimal binding to these proteins being retained. Finally, only commercially available compounds with ≥90% purity were selected for *in vitro* validation and *Drosophila* model testing. B) Chemical structures of the five phytochemicals identified through screening and subsequently investigated *in vitro* and *in vivo* in this study.

Figure 2 *In vitro* validation of ERO1A inhibitory activity. A) Schematic representation of the ERO1A–PDI oxidoreductase reaction. ERO1A catalyzes the oxidation of PDI, generating hydrogen peroxide (H_2O_2) as a by-product. In the presence of H_2O_2, horseradish peroxidase (HRP) converts Amplex® UltraRed (AUR) into the fluorescent product resorufin, allowing quantification of ERO1A activity. B) Fluorescence intensity measured in the presence or absence of selected phytochemicals or the known ERO1A inhibitor EN460. Fluorescence was measured every 10 minutes over a 30-minute period with excitation at 544 nm and emission at 590 nm (top read). C) Percentage of ERO1A enzymatic activity recorded after 10 minutes of pre-incubation. Activity in the presence of each inhibitor was calculated relative to the uninhibited control condition (set at 100%). Data represent the mean ± SEM of three independent experiments.

Figure 3 Identified phytochemicals retain ERO1 inhibitory properties *in vivo*. (A–E) Survival curves, analysed using the Log-rank (Mantel-Cox) test, show pan-neuronal (nSyb-GAL4) ERO1L-overexpressing flies treated with increasing doses (1, 5, or 10 μM) of S43 (A), S47 (B), S76 (C), S88 (D), and T2212 (E), respectively, or left untreated (standard food containing vehicle). An inset for each phytochemical treatment displays the quartile percentage of mortality at each tested dose. The median survival of untreated nSyb>ERO1L flies is 24 days, and a dotted line has been overlaid on each graph to facilitate visualization of the phytochemical treatments' effects in mitigating the toxicity of elevated ERO1L expression in neurons. F) The bar chart presents the highest recorded median survival of nSyb>ERO1L flies following phytochemical treatment. The *in vivo* ERO1L inhibitory activity of the identified phytochemicals is compared to that of EN460, whose complete survival curve is shown in Supplementary Figure S1.

Figure 4 The administration of S88 or T2212 does not induce toxicity in primary cells or cell lines. A) Experimental design scheme. B-F”) Cell viability of human-derived fibroblast (HDF) (B-F), Hep2G (B'-F'), and SH-SY5Y (B''-F'') cells after 48 hour (h) incubation with increasing concentrations of identified phytochemicals (0 to 20 μM). Cell viability was assessed using the MTT assay, with viability data compared to untreated or vehicle (0.1% DMSO) treated controls. The data illustrate the effects of progressive concentration increases on cell viability across the different cell types.

Statistical significance was determined using one-way ANOVA, with a significance threshold set at *$p < 0.05$. The data related to cell viability after 24h phytochemical treatment are shown in Supplementary Figure S2.

Figure 5 S88 and T2212 enhance viability and reduce ER stress markers in Tm-stressed SH-SY5Y cells. A) Experimental design with undifferentiated SH-SY5Y cells. B) Expression levels of ER stress markers in Tm 1 µM (Tm-1)-stressed SH-SY5Y cells after 24 hours (h) phytochemical (phyto) administration at 20 µM. Dose- and time-dependent response of Tm-1-stressed undifferentiated SH-SY5Y cells is shown in Supplementary Figure S3. C) Experimental design with Retinoic acid (RA)-differentiated SH-SY5Y cells. D-E) Cell viability of SH-SY5Y cells Tm-1 stressed for 24h, followed by 24h treatment with increasing concentration of either S88 (D) or T2212 (E) in continue presence of Tm-1. Cell viability was measured using the MTT assay and compared to vehicle (0.1% DMSO) controls. F-J) Crude extracts from Tm-1 stressed cells with or without phytochemical treatment (1 or 2.5 µM) were examined by immunoblot analysis with the indicated antibodies. Levels of ER stress markers were compared with that of unstressed cells. β-tubulin was used as endogenous control. Statistical significance was determined using one-way ANOVA, with a significance threshold set at *$p < 0.05$.

Figure 6 S88 and T2212 improve early neuronal health in UBQLN2^{ALS} models, but only S88 sustains late-stage locomotor benefits A) Experimental design. B) Larval movement was quantified by measuring the total distance travelled within 30 seconds (sec), presented as a scatter plot with geometric mean. (C) Representative locomotor trajectories for each genotype tested. D) Type I motor neurons (Ib MNs4) innervating muscle 4 in larvae expressing UBQLN2^{ALS} under elav-GAL4 (*elav> UBQLN2^{ALS}*) were immunostained for the presynaptic membrane marker horseradish peroxidase (HRP, green) and the postsynaptic marker Discs large (Dlg). Larvae were either untreated (vehicle, veh) or treated with different concentrations of S88 or T2212. Scale bars: 50 µm. Single fluorescent channels and additional representative NMJ are shown in Supplementary Figure S8 and S9. (E) Branch length and (F) synaptic bouton number were quantified using ImageJ v.1.53k, with data displayed as box and violin plots. (G) Locomotor functions in adult *elav> UBQLN2^{ALS}* flies were assessed using a climbing assay. Flies were either untreated (veh, n = 127) or treated with varying concentrations of S88 (n = 103) or T2212 (n = 112). Climbing performance was recorded at 5, 10, 15, 20, 25, and 30 days post-eclosion, with scores compared across age-matched groups. Statistical analysis was conducted using one-way ANOVA followed by Dunnett’s test for crawling and NMJ assessments, while two-way ANOVA with Tukey’s multiple comparisons test was applied for the climbing assay. Statistical significance was considered at *$p < 0.05$.

Figure 7 Efficacy of S88 in late-stage UBQLN2^{ALS} flies is associated with reduced p-eIF2α but sustained ATF4 levels. A) Schematic representation of disease progression and time points for ER stress marker analysis. (B-I) Immunoblots analysis of crude extracts from (B-E) larval brains (early stage of disease) or (F-I) 30 days-old (D30) (late stage of disease) heads of flies treated with either S88 or T2212 or left untreated (UNT). ER stress marker levels were compared to age-matched untreated controls. UBQLN2 levels were also assessed across treatment groups. Actin or β-tubulin were used as loading controls. Statistical significance was determined using one-way ANOVA with a threshold of *$p < 0.05$.

Figure 8 Pharmacological intervention with S88 improves survival in a *Drosophila* model of D-GAL–induced accelerated aging. Survival curves of the *Drosophila* aging model induced by dietary D-galactose (DG25), treated with increasing concentrations (1 or 5 µM) of S88 (A) or T2212 (B), or left untreated. For reference, survival of control flies raised on standard food containing vehicle (DG0) is also shown. Median survival of the DG25 group is indicated by the grey dotted line in both panels. Statistical analysis was performed using the Log-rank (Mantel-Cox) test, with significance defined as $p < 0.05$. The dose-dependent effect of D-GAL on *Drosophila* lifespan is shown in Supplementary Figure S12.

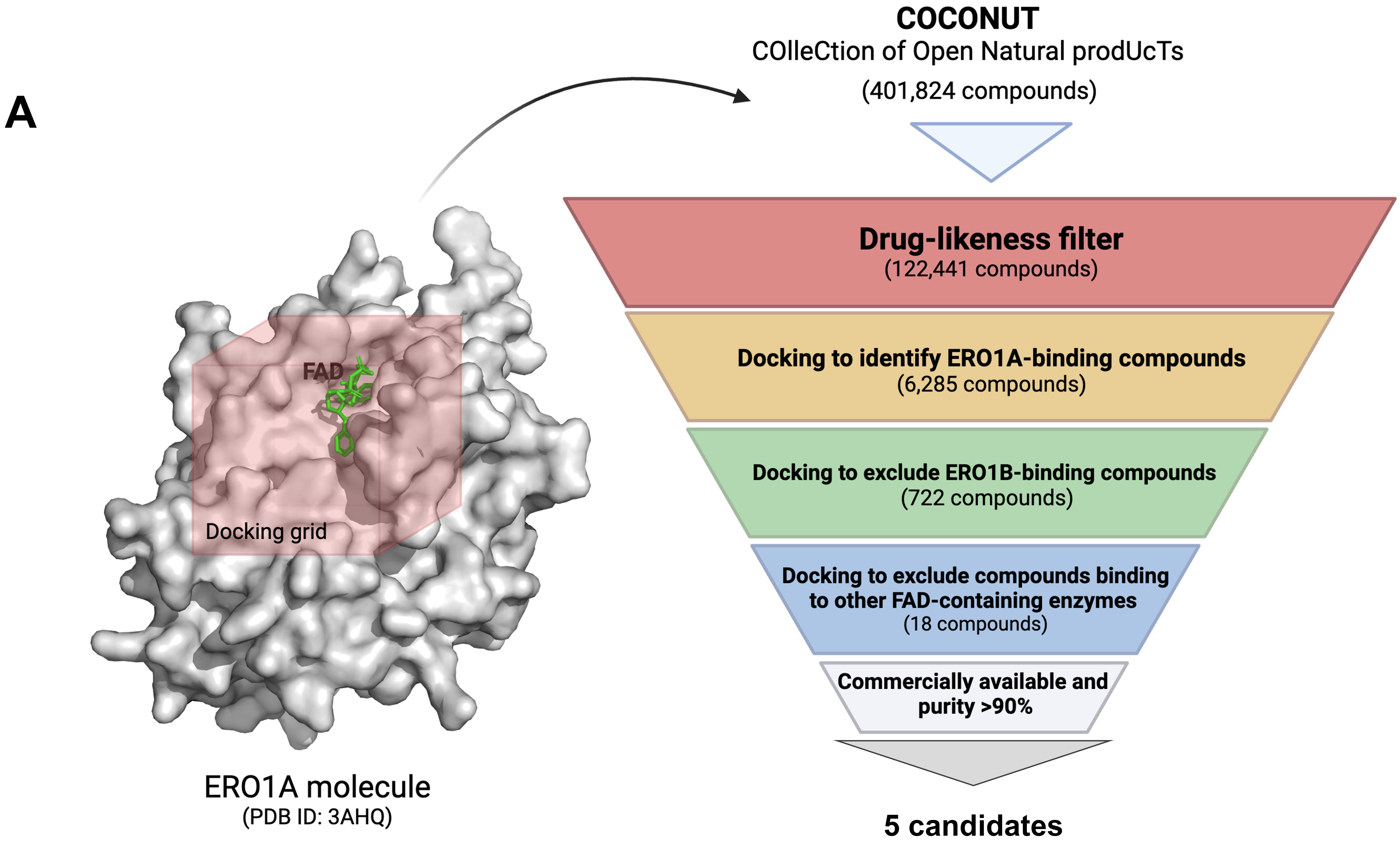
A
COCONUT
COlleCtion of Open Natural prodUcTs
(401,824 compounds)
Drug-likeness filter
(122,441 compounds)
Docking to identify ERO1A-binding compounds
(6,285 compounds)
Docking to exclude ERO1B-binding compounds
(722 compounds)
Docking to exclude compounds binding to other FAD-containing enzymes
(18 compounds)
Commercially available and purity >90%
5 candidates
FAD
Docking grid
ERO1A molecule
(PDB ID: 3AHQ)

B

N-(2-hydroxyethyl)-2-[(3,4,8,8-tetramethyl-2-oxo-9,10-dihydro-2H,8Hpyrano[2,3-f]chromen-5-yl)oxy]acetamide

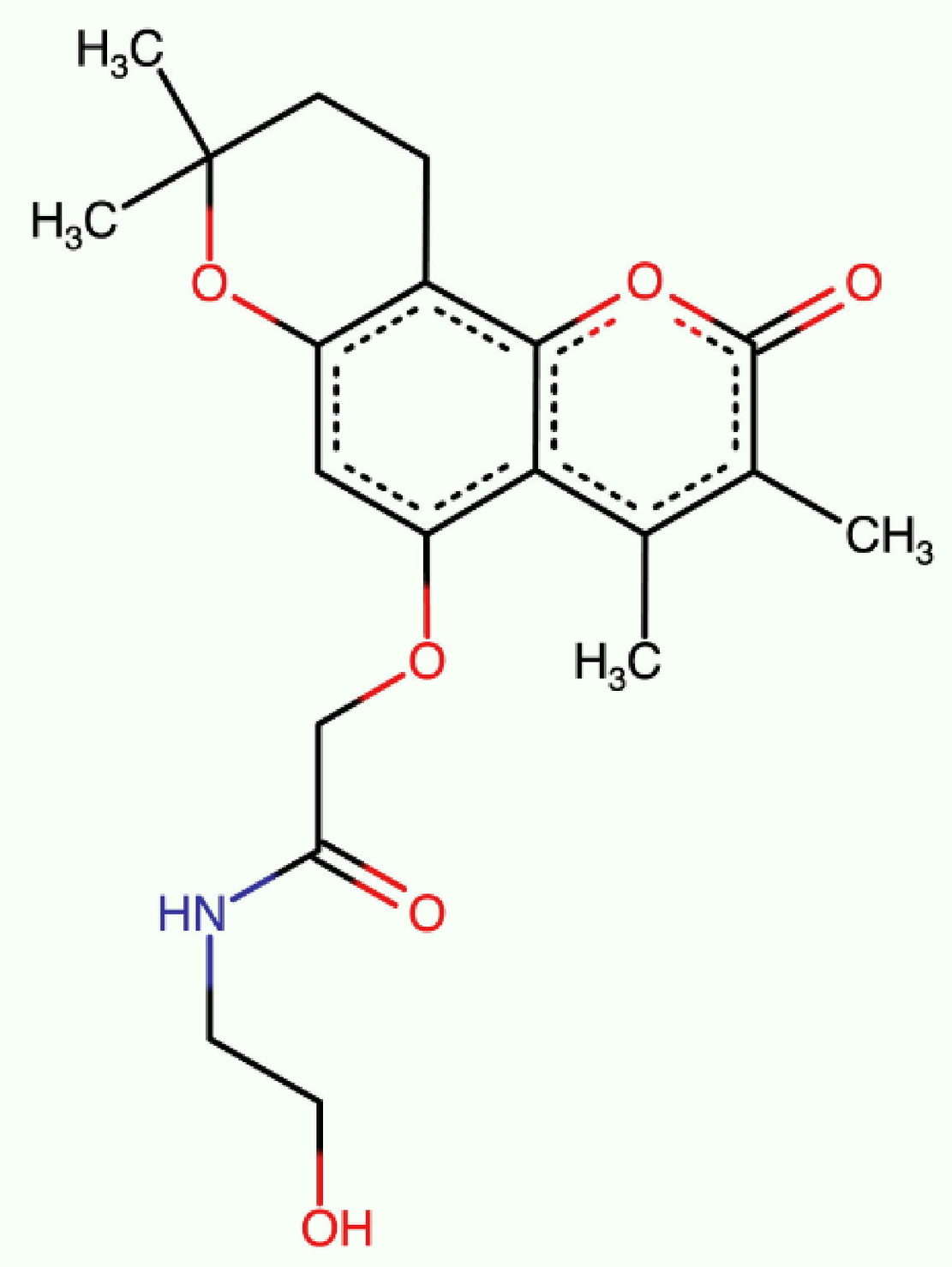
H3C
H3C
O
O
O
CH3
H3C
O
HN
O
OH

STL522543 (S43)

4-(4-hydroxy-3,5-dimethoxyphenyl)-7,7-dimethyl-4,6,7,8-tetrahydro-2Hchromene-2,5(3H)-dione

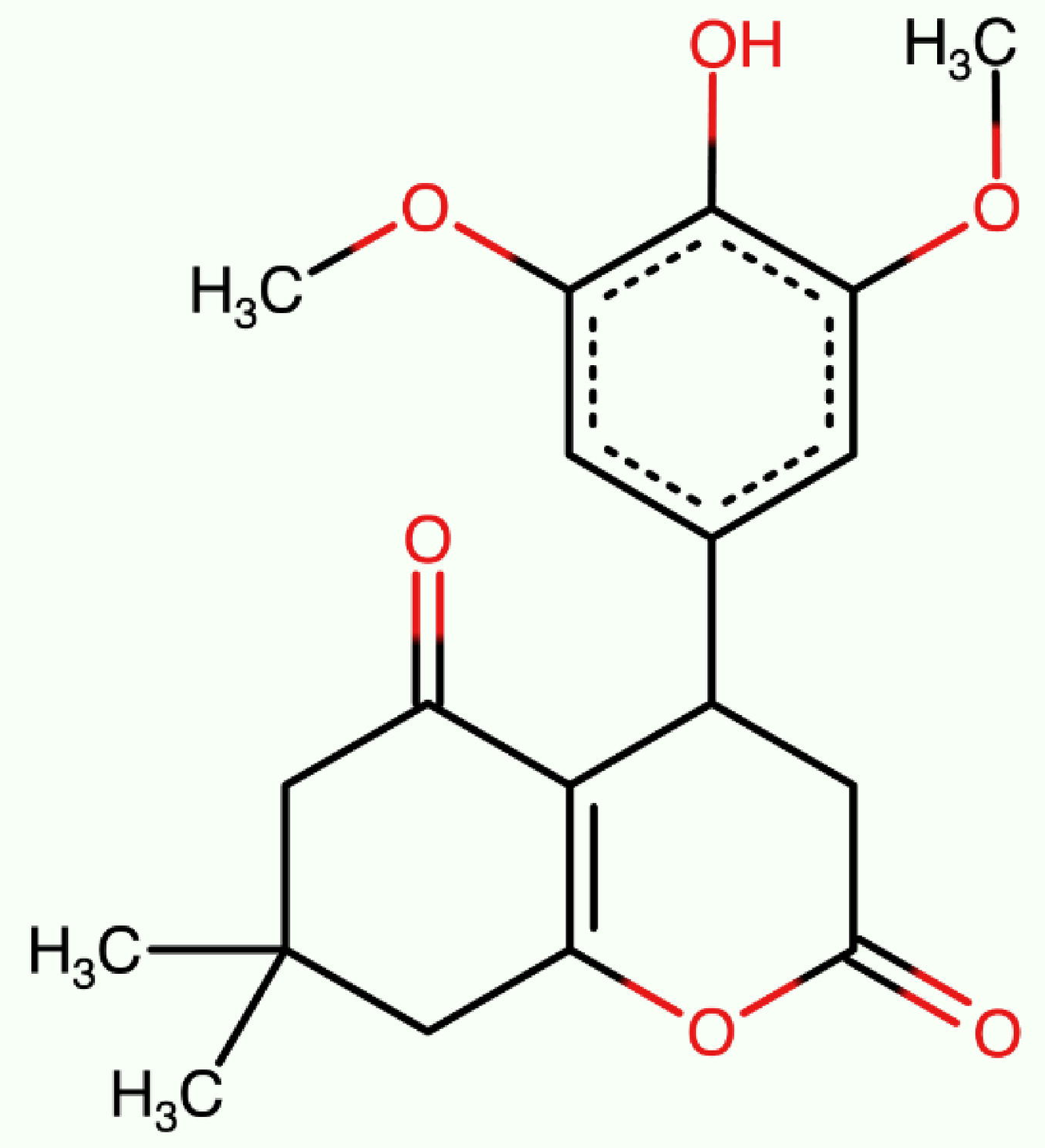
OH
H3C
O
H3C
O
O
H3C
H3C
O
O

STL551047 (S47)

(2E)-3-(3,5-di-tert-butyl-4-hydroxyphenyl)prop-2-enoicacid

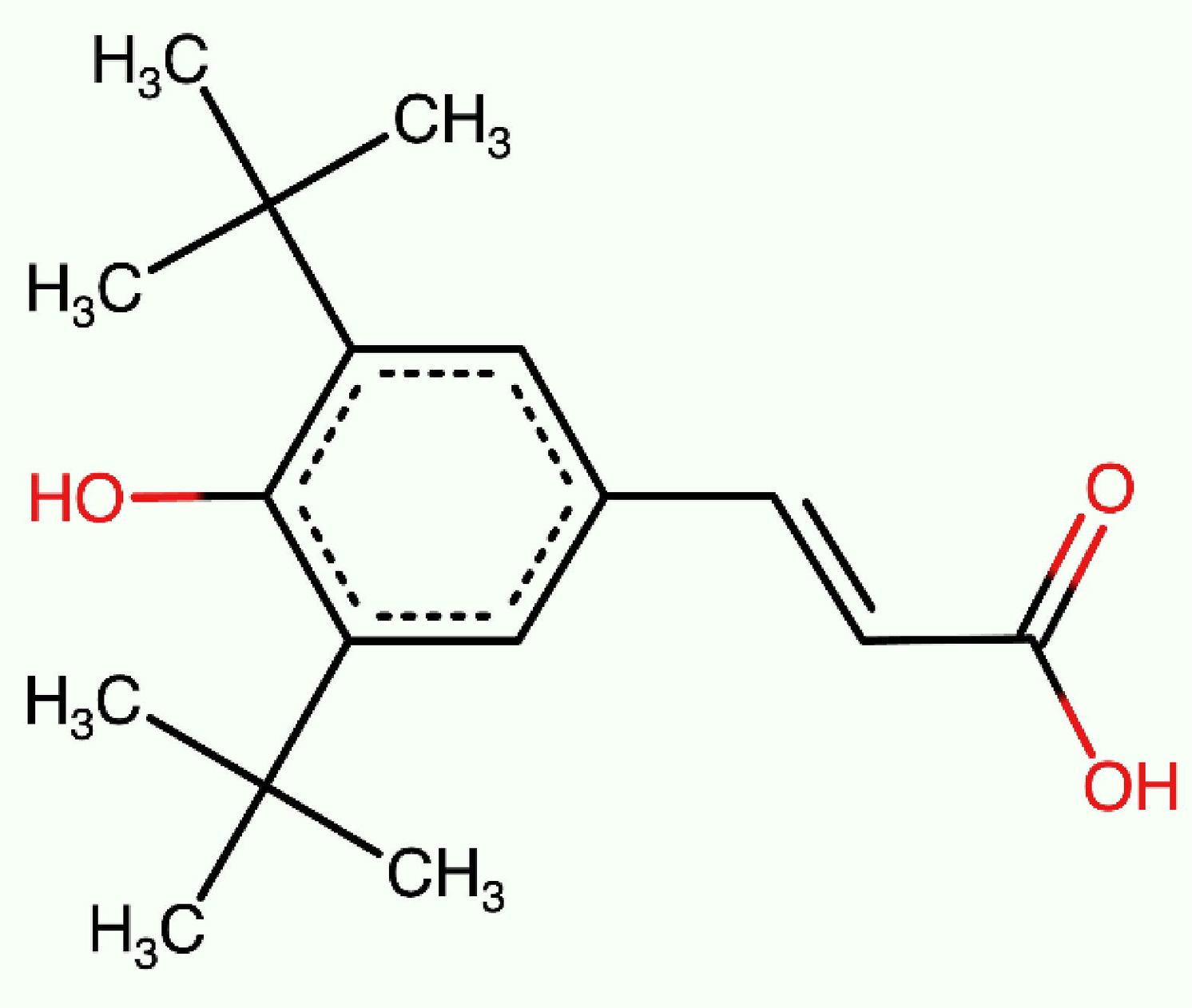
H3C
CH3
H3C
HO
O
H3C
OH
H3C
CH3

STK179676 (S76)

methyl3-hydroxy-5-{3-methyl-1-oxo-1-[(1S,5R)-8-oxo-1,5,6,8-tetrahydro-2H -1,5-methanopyrido[1,2-a][1,5]diazocin-3(4H)-yl]butan-2-yl}-5Hpyrazolo[4,3-c]pyridine-7-carboxylate

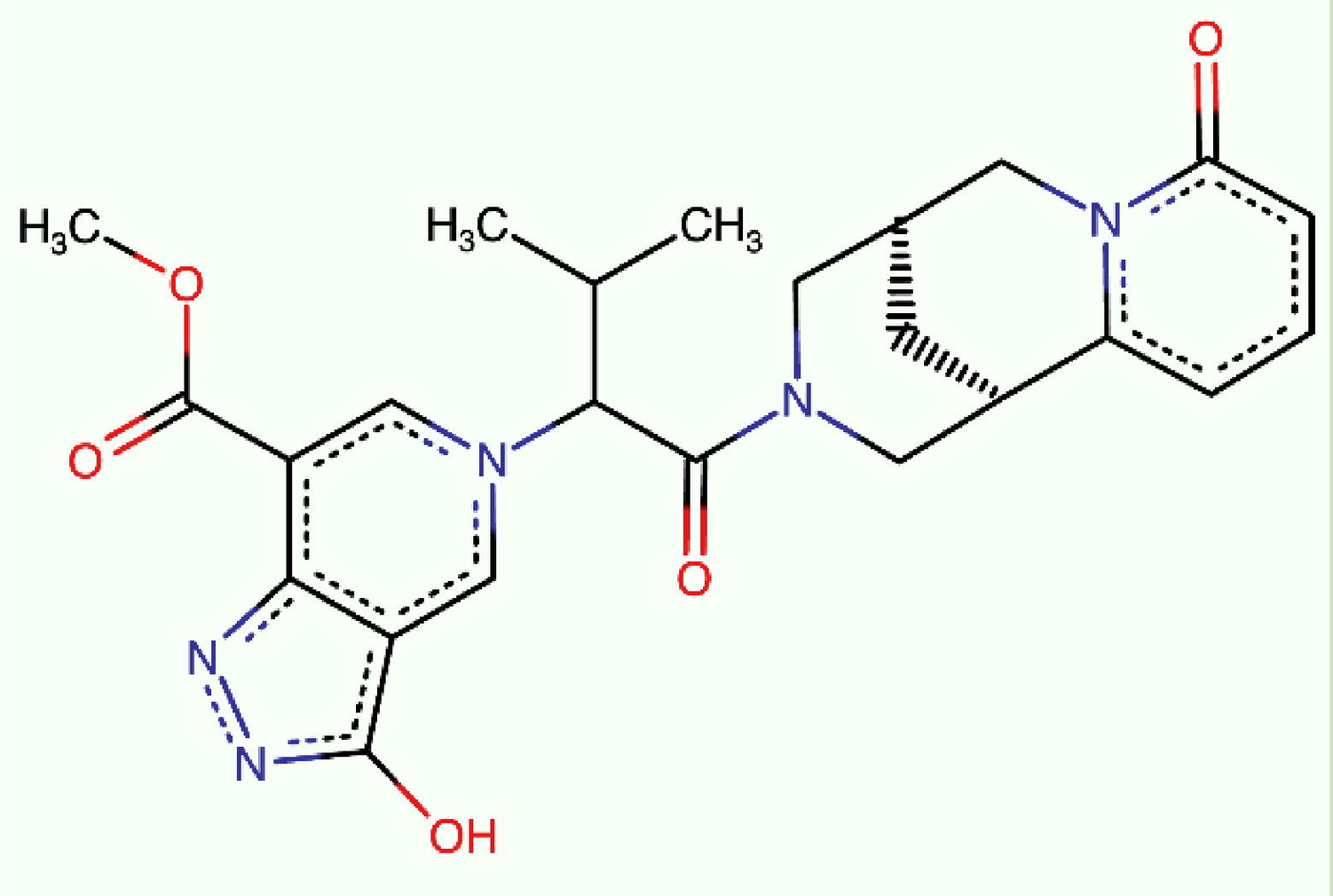
H3C
O
O
H3C
CH3
N
O
N
N
O
N
N
OH

STL546888 (S88)

methyl1-(hexopyranosyloxy)-7-(hydroxymethyl)-1, 4a,5,7 atetrahydrocyclopenta[c]pyran-4-carboxylate

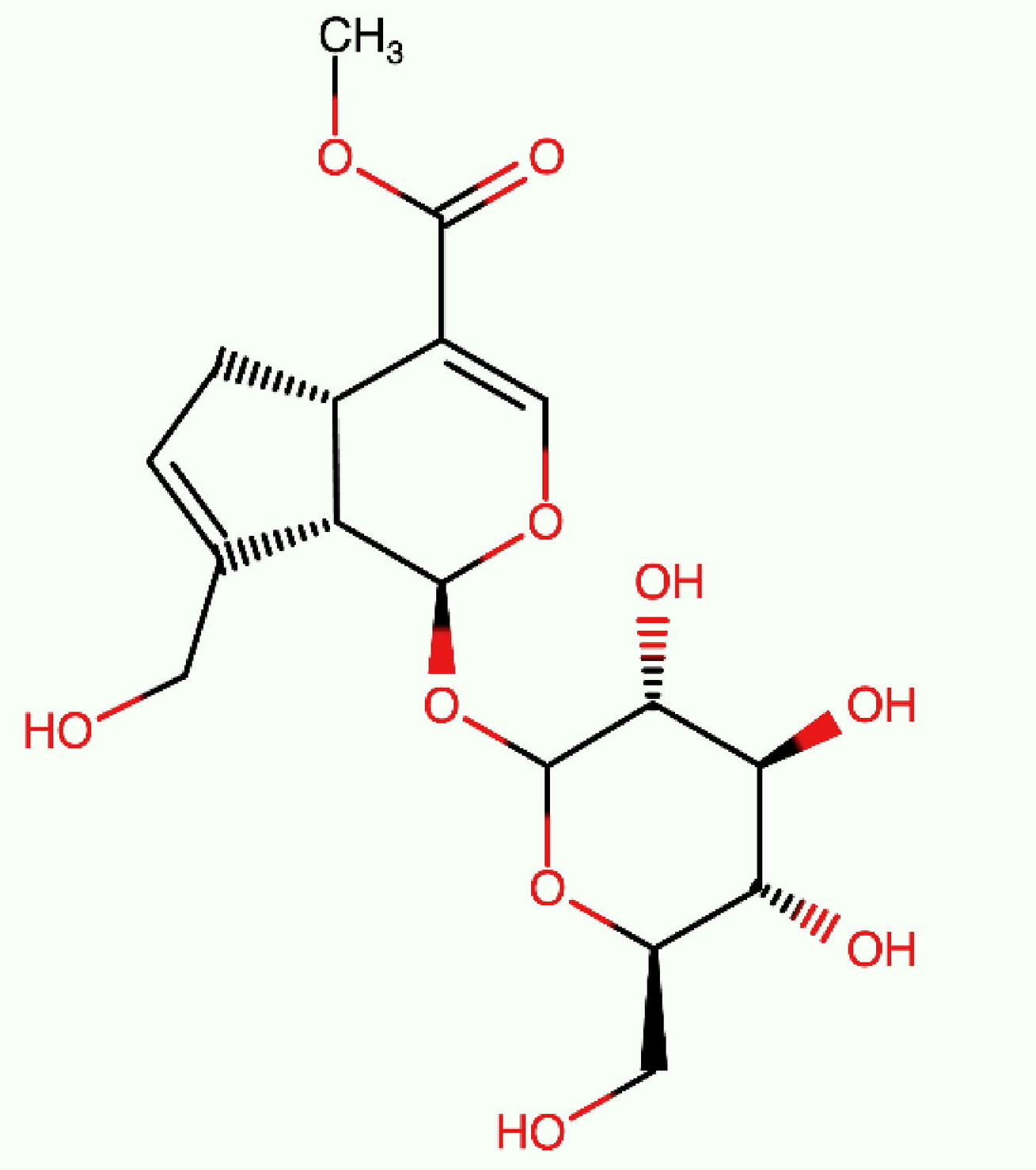
CH3
O
O
O
HO
O
OH
OH
O
OH
HO

geniposide (T2212)

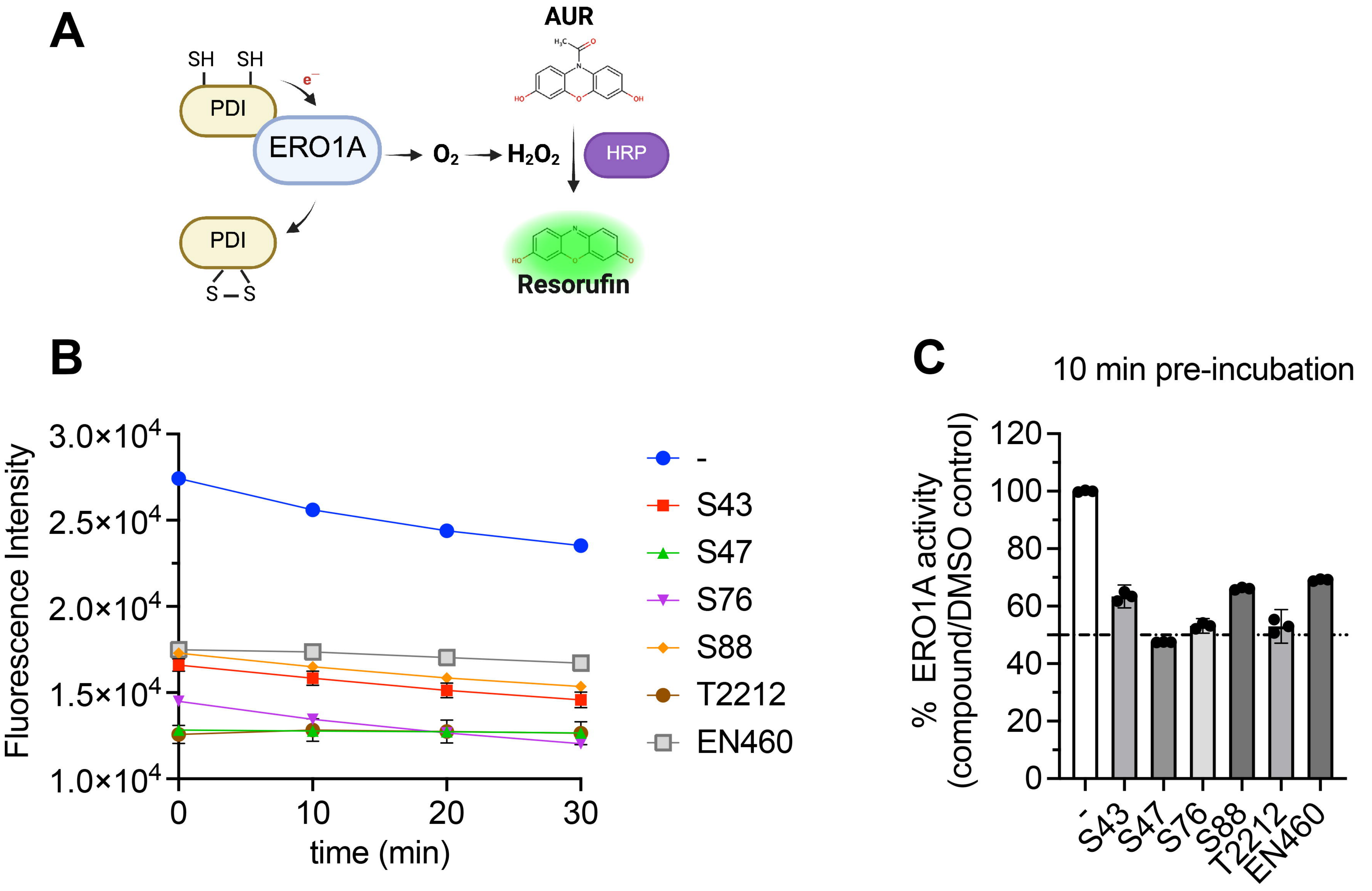
A
SH SH
PDI
e⁻
ERO1A
O2
H2O2
AUR
HRP
PDI
S–S
Resorufin
B
Fluorescence Intensity
3.0×10^4
2.5×10^4
2.0×10^4
1.5×10^4
1.0×10^4
0
10
20
30
time (min)
-
S43
S47
S76
S88
T2212
EN460
C
10 min pre-incubation
% ERO1A activity (compound/DMSO control)
120
100
80
60
40
20
0
-
S43
S47
S76
S88
T2212
EN460

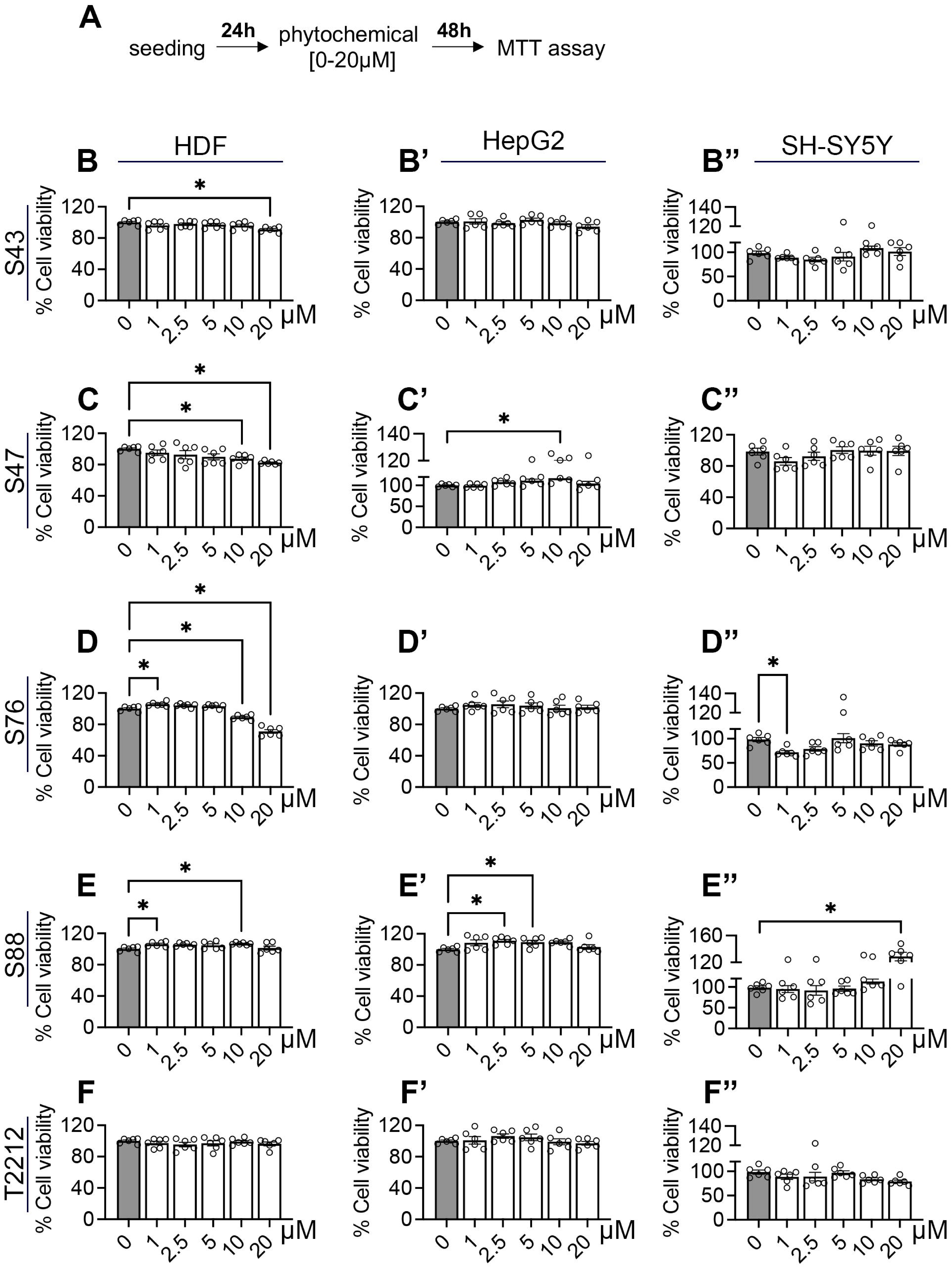
A
seeding
24h
phytochemical [0-20µM]
48h
MTT assay
HDF
HepG2
SH-SY5Y
B
B'
B"
C
C'
C"
D
D'
D"
E
E'
E"
F
F'
F"
S43
S47
S76
S88
T2212
% Cell viability
0
1
2.5
5
10
20
µM
*

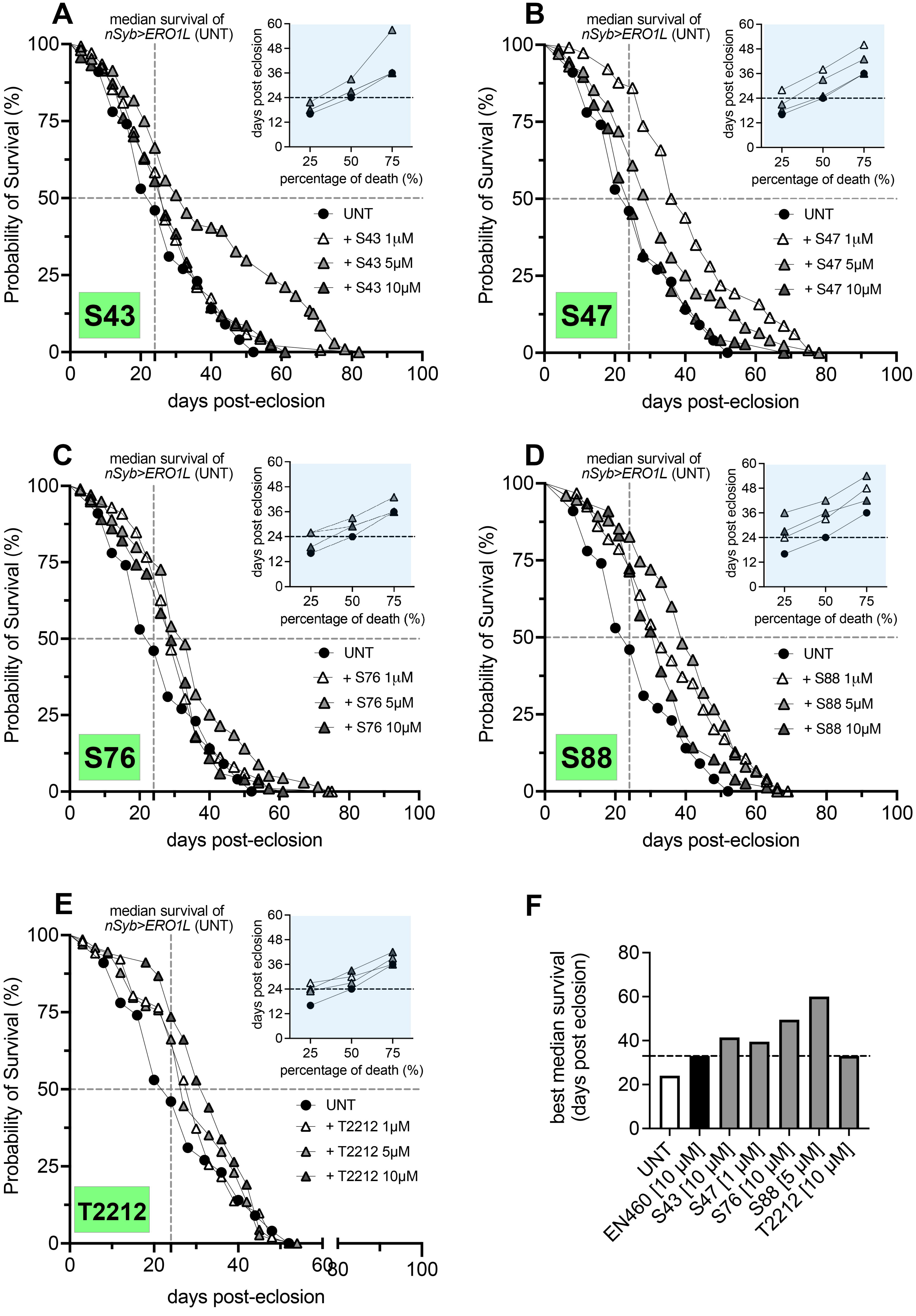
A
median survival of
nSyb>ERO1L (UNT)
Probability of Survival (%)
0
25
50
75
100
days post-eclosion
0
20
40
60
80
100
days post eclosion
percentage of death (%)
25
50
75
0
12
24
36
48
60
UNT
+ S43 1μM
+ S43 5μM
+ S43 10μM
S43
B
median survival of
nSyb>ERO1L (UNT)
UNT
+ S47 1μM
+ S47 5μM
+ S47 10μM
S47
C
median survival of
nSyb>ERO1L (UNT)
UNT
+ S76 1μM
+ S76 5μM
+ S76 10μM
S76
D
median survival of
nSyb>ERO1L (UNT)
UNT
+ S88 1μM
+ S88 5μM
+ S88 10μM
S88
E
median survival of
nSyb>ERO1L (UNT)
UNT
+ T2212 1μM
+ T2212 5μM
+ T2212 10μM
T2212
F
best median survival
(days post eclosion)
0
20
40
60
80
UNT
EN460 [10 μM]
S43 [10 μM]
S47 [1 μM]
S76 [10 μM]
S88 [5 μM]
T2212 [10 μM]

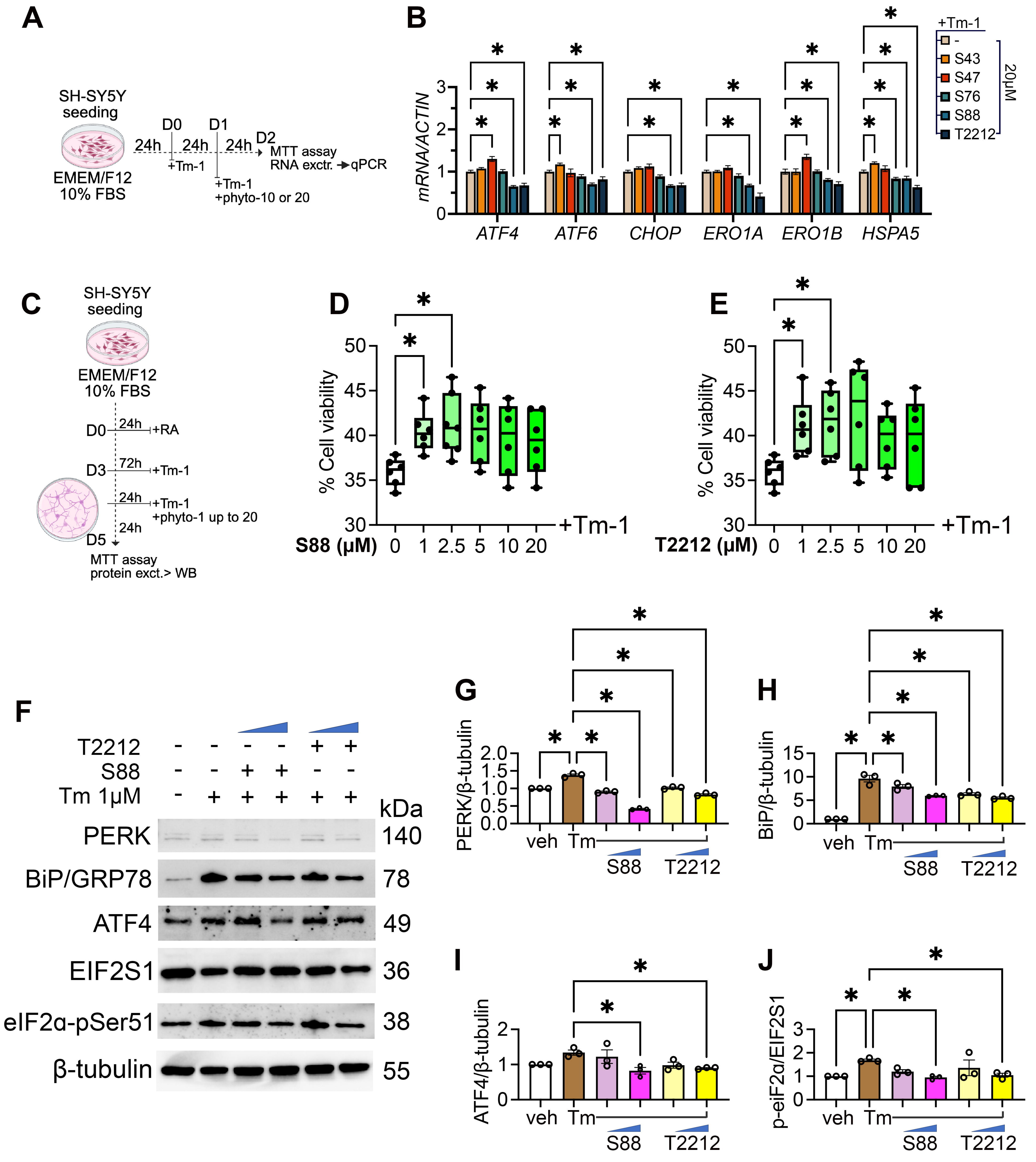
A
SH-SY5Y seeding
EMEM/F12 10% FBS
24h
D0
24h
D1
24h
D2
+Tm-1
+Tm-1
+phyto-10 or 20
MTT assay
RNA exctr. → qPCR
B
mRNA/ACTIN
0
1
2
3
ATF4
ATF6
CHOP
ERO1A
ERO1B
HSPA5
*
+Tm-1
-
S43
S47
S76
S88
T2212
20μM
C
SH-SY5Y seeding
EMEM/F12 10% FBS
D0
24h
+RA
D3
72h
+Tm-1
24h
+Tm-1
+phyto-1 up to 20
24h
D5
MTT assay
protein exct.> WB
D
% Cell viability
30
35
40
45
50
S88 (μM)
0
1
2.5
5
10
20
+Tm-1
*
E
% Cell viability
30
35
40
45
50
T2212 (μM)
0
1
2.5
5
10
20
+Tm-1
*
F
T2212
S88
Tm 1μM
kDa
PERK
140
BiP/GRP78
78
ATF4
49
EIF2S1
36
eIF2α-pSer51
38
β-tubulin
55
G
PERK/β-tubulin
0.0
0.5
1.0
1.5
2.0
veh
Tm
S88
T2212
*
H
BiP/β-tubulin
0
5
10
15
veh
Tm
S88
T2212
*
I
ATF4/β-tubulin
0
1
2
veh
Tm
S88
T2212
*
J
p-eiF2α/EIF2S1
0
1
2
3
veh
Tm
S88
T2212
*

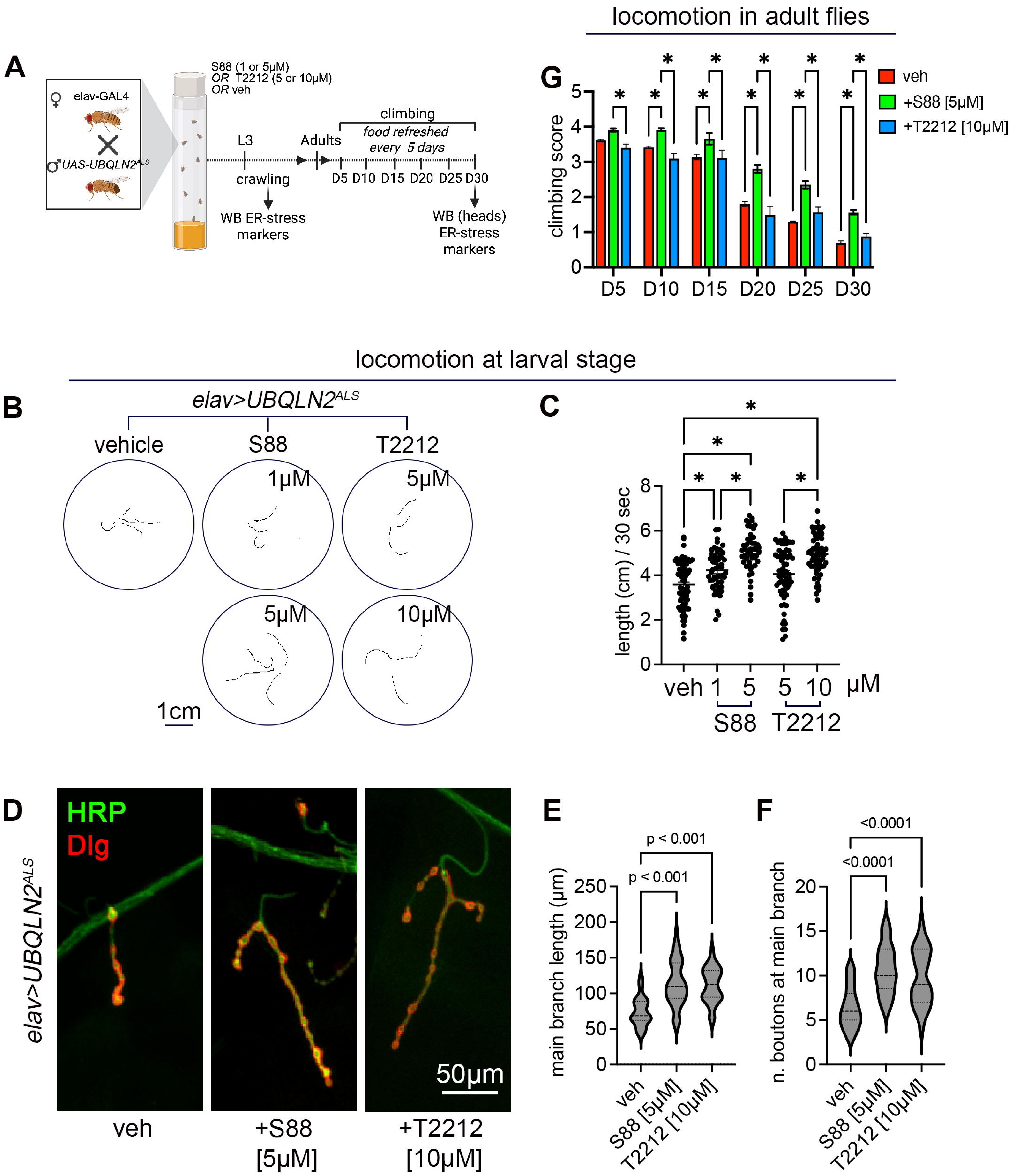
locomotion in adult flies
A
♀ elav-GAL4
♂ UAS-UBQLN2ALS
S88 (1 or 5µM)
OR T2212 (5 or 10µM)
OR veh
L3
crawling
WB ER-stress markers
Adults
climbing
food refreshed every 5 days
D5 D10 D15 D20 D25 D30
WB (heads) ER-stress markers
G
climbing score
0 1 2 3 4 5
D5 D10 D15 D20 D25 D30
*
🟥 veh
🟩 +S88 [5µM]
🟦 +T2212 [10µM]
locomotion at larval stage
B
elav>UBQLN2ALS
vehicle
S88
T2212
1µM
5µM
5µM
10µM
1cm
C
length (cm) / 30 sec
0 2 4 6 8
veh 1 5 5 10 µM
S88
T2212
*
D
HRP
Dlg
elav>UBQLN2ALS
50µm
veh
+S88 [5µM]
+T2212 [10µM]
E
main branch length (µm)
0 50 100 150 200 250
p < 0.001
p < 0.001
veh
S88 [5µM]
T2212 [10µM]
F
n. boutons at main branch
0 5 10 15 20
<0.0001
<0.0001
veh
S88 [5µM]
T2212 [10µM]

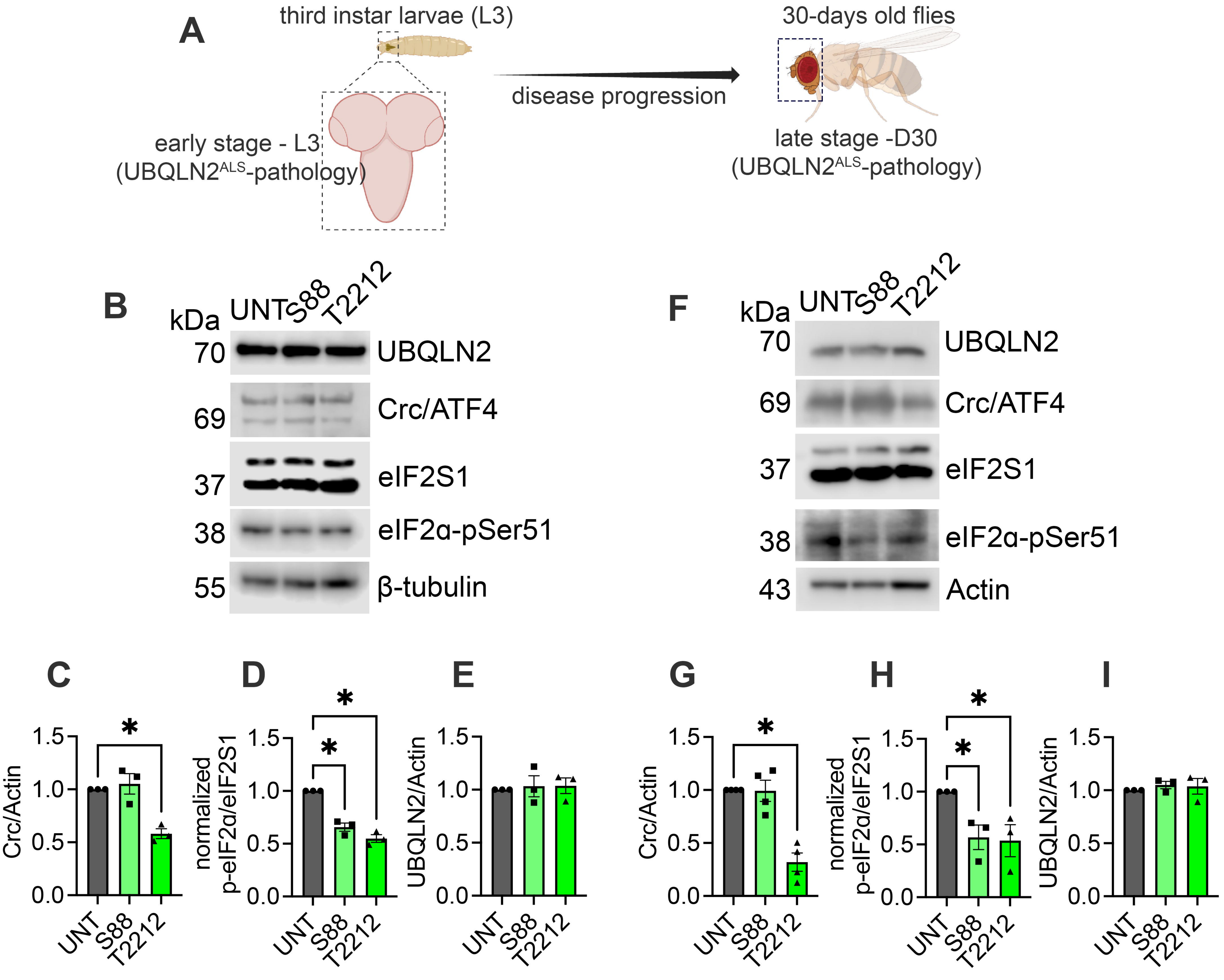
A
third instar larvae (L3)
early stage - L3
(UBQLN2^{ALS}-pathology)
disease progression
30-days old flies
late stage -D30
(UBQLN2^{ALS}-pathology)
B
kDa
UNT
S88
T2212
70
UBQLN2
69
Crc/ATF4
37
eIF2S1
38
eIF2α-pSer51
55
β-tubulin
F
kDa
UNT
S88
T2212
70
UBQLN2
69
Crc/ATF4
37
eIF2S1
38
eIF2α-pSer51
43
Actin
C
Crc/Actin
1.5
1.0
0.5
0.0
*
UNT
S88
T2212
D
normalized p-eIF2α/eIF2S1
1.5
1.0
0.5
0.0
*
*
UNT
S88
T2212
E
UBQLN2/Actin
1.5
1.0
0.5
0.0
UNT
S88
T2212
G
Crc/Actin
1.5
1.0
0.5
0.0
*
UNT
S88
T2212
H
normalized p-eIF2α/eIF2S1
1.5
1.0
0.5
0.0
*
*
UNT
S88
T2212
I
UBQLN2/Actin
1.5
1.0
0.5
0.0
UNT
S88
T2212

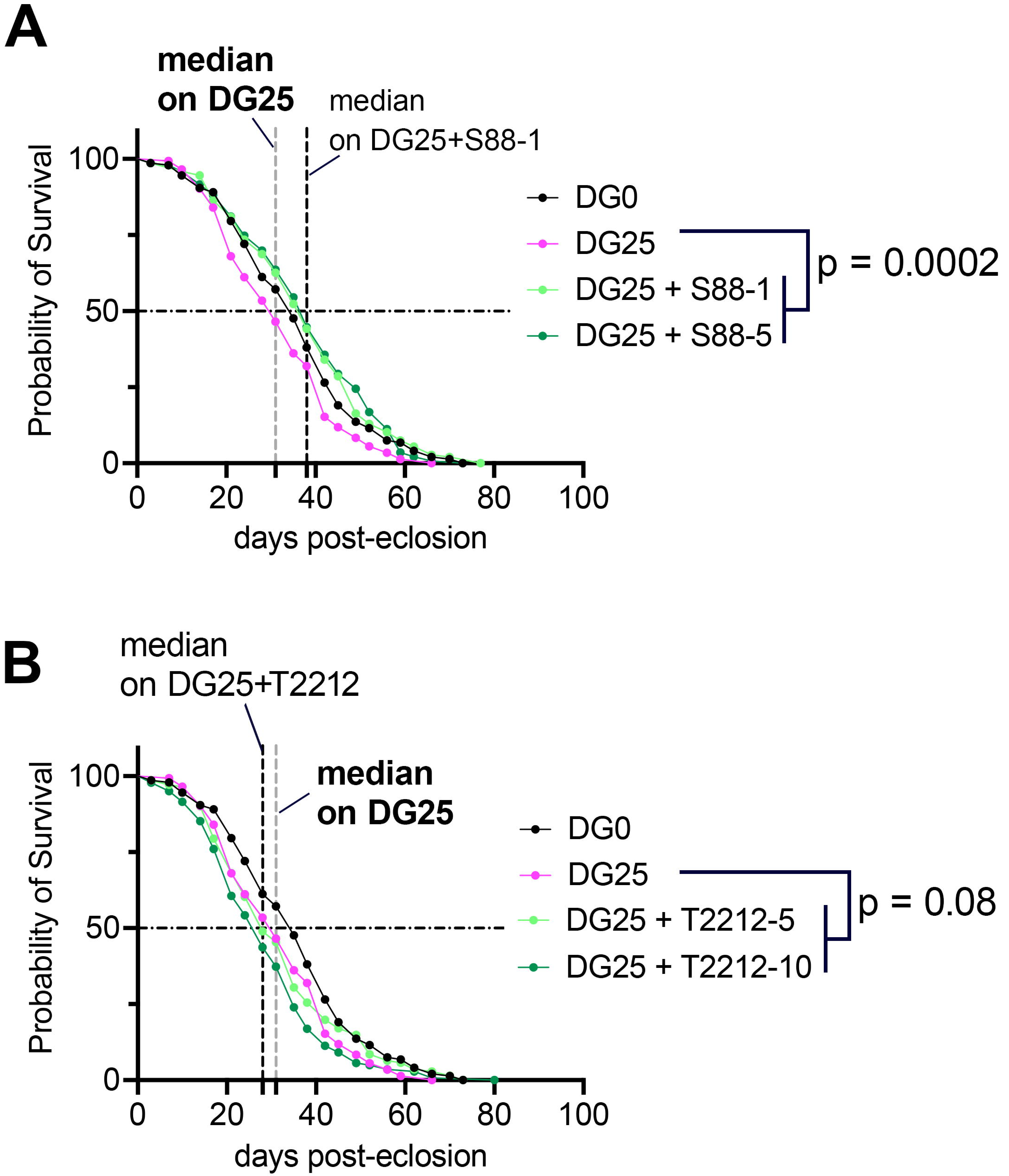
A
median
on DG25
median
on DG25+S88-1
Probability of Survival
100
50
0
0
20
40
60
80
100
days post-eclosion
DG0
DG25
DG25 + S88-1
DG25 + S88-5
p = 0.0002
B
median
on DG25+T2212
median
on DG25
Probability of Survival
100
50
0
0
20
40
60
80
100
days post-eclosion
DG0
DG25
DG25 + T2212-5
DG25 + T2212-10
p = 0.08